Fluorescence and magnetic resonance spectra of Nd^{3+} and Er^{3+} ions in single crystals of $LaCl_3$

Clyde A. Hutchison Jr., Steven G. Utterback,* and Philip M. Martineau†
Enrico Fermi Institute and Department of Chemistry, The University of Chicago, Chicago, Illinois 60637
(Received 25 April 1988)

This article presents the results of experiments in which the 19 429.67-cm^{-1} emission of an Ar^+ laser is used to pump the Z_1, $^4I_{9/2}$, $\mu=\frac{5}{2}\rightarrow F_1$, $^2G_{9/2}$, $\mu=\frac{1}{2}$ transition of Nd^{3+} ions dilutely substituted at La^{3+} sites in $LaCl_3$ crystals in an $\sim$1.6-K bath of liquid He. In some of the work Er^{3+} ions are also present. When an external magnetic field is applied electron paramagnetic resonance (EPR) absorption of microwave energy by either Nd^{3+} or Er^{3+} results in marked intensity changes of Nd^{3+} fluorescence emissions. The essential new feature of this work is the observation of the importance of the effects of the heating of the crystal above the bath temperature by both optical and microwave absorption. The heating by phonons generated in the radiationless transitions associated with the optical pumping cycle results in the emission of 17 E and D Nd^{3+} fluorescences not observed in previous work with the crystal at $\sim$1.6 K. Because of the encapsulation of the crystals in silica envelopes in these experiments, the heating effects are especially marked at higher laser powers. These new fluorescences result from the state population redistributions effected by the rise in temperature of the crystal. EPR microwave absorption by either Nd^{3+} or Er^{3+} accompanied by spin-lattice relaxation results in a further increase in crystal temperature and further Nd^{3+} state population redistributions with concommitant changes in the intensities of the fluorescence emissions from these states of Nd^{3+}. This affords a new mechanism for optically detected magnetic resonance (ODMR) of these rare-earth ions. This new mechanism for ODMR produces optical signals strikingly different from those previously studied which result from the changes in the populations of the two components of the ground Z_1 doublet of Nd^{3+} produced by Z_1 microwave absorption or by microwave absorption by the Er^{3+} ground doublet with subsequent transfer of Zeeman quanta between Er^{3+} and Nd^{3+} and resultant changes in optical pumping rates and fluorescence emissions. The factors contributing to the new mechanism for ODMR also account for the observed changes with temperature in the characters of the decays of the ODMR signals when microwave irradiation is terminated. With constant intensity laser irradiation in the absence of external magnetic fields the 28 observed fluorescence emissions oscillate in synchrony at frequencies $\frac{1}{2}$ to $\frac{1}{3}$ Hz, when the laser irradiation intensity lies in a certain narrow range. Several mechanisms considered as explanations of this phenomenon have failed to account for its observed features. It is clear, however, that these oscillations of emission intensity are accompanied by oscillations in the temperature of the crystal and of the populations of the emitting states.

I. INTRODUCTION

We report studies of relationships between the fluorescence emissions of Nd^{3+} ions and the EPR (electronic paramagnetic resonance) absorptions of Nd^{3+} and Er^{3+} ions when these ions are dilutely substituted at La^{3+} sites with C_{3h} point symmetry in the anhydrous hexagonal $LaCl_3$ crystal.[1,2] In the course of this work we have observed (a) a new mechanism for the optically detected magnetic resonance (ODMR) of rare-earth ions, (b) 17 previously unobserved fluorescence emissions associated with this mechanism, and (c) temporal oscillations of the intensities of the fluorescences during constant intensity optical irradiation of the $LaCl_3$ crystal.

The sharp line fluorescence spectra of Nd^{3+} and Er^{3+} in $LaCl_3$ have been thoroughly investigated by Dieke and co-workers[3–7] and by others.[8–13] The electron paramagnetic resonance (EPR) and electron nuclear double resonance (ENDOR) of these ions in $LaCl_3$ in both their ground and excited states and as both isolated ions and juxtaposed pairs of ions, have been extensively studied in our laboratory.[14–18] We have also investigated the ODMR of Nd^{3+} and Er^{3+} and the transfer of ground-state Zeeman quanta between them in the $LaCl_3$ crystal.[19–21] Our knowledge of the excited states and their energies in the $LaCl_3$ crystal, crucial for the understanding of the magnetic resonance observations, derives mainly from the optical studies by Dieke and co-workers.[3–7] The crystal-field electronic energy levels are shown in Figs. 1–3. The EPR spectrum of $^{144}Nd^{3+}$ (zero nuclear spin) ions dilutely substituted at La^{3+} sites in $LaCl_3$ is well described by the spin Hamiltonian

$$\mathcal{H}=|\mu_B|\mathbf{B}_0\cdot\vec{\mathbf{g}}\cdot\mathcal{S},\quad S=\tfrac{1}{2}\ . \tag{1}$$

The principal values of $\vec{\mathbf{g}}$, together with those for Er^{3+}, are given in Table I. An understanding of the results reported here requires the immediately following brief review of previous work in our laboratory.

In our earlier work, and also in the work reported here,

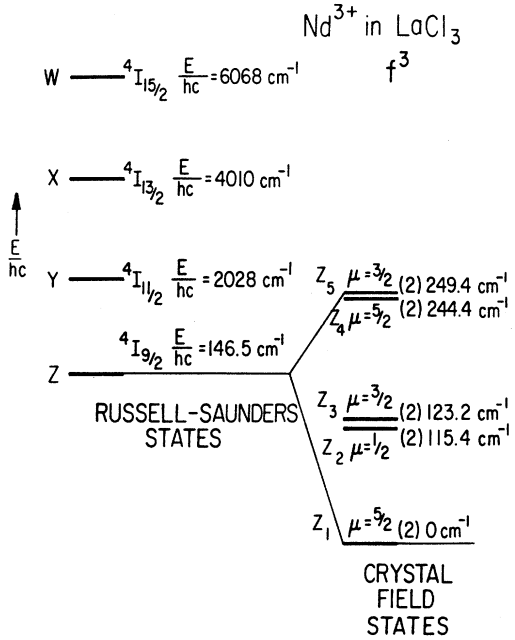

FIG. 1. Energy levels of the ^4I ground manifold of Nd^{3+} in the $LaCl_3$ crystal. The numerical values are from Dieke (Ref. 4) and his symbolism is used.

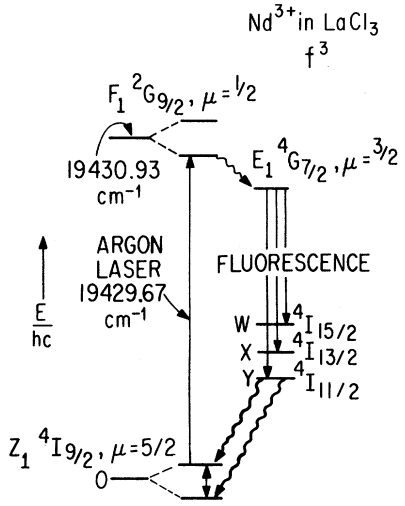

FIG. 2. Optical pumping cycles for the populating of the crystal-field states of lowest energy for $^4I_{15/2}$, $^4I_{13/2}$, and $^4I_{11/2}$ terms of Nd^{3+} in the $LaCl_3$ crystal. The numerical value for F_1 is from Dieke (Ref. 4) and his symbolism is used.

with the crystal at temperature, ~ 1.6 K, we used the Ar^+-laser emission at 19 429.67 cm^{-1} to pump the transition,

$$Z_1,\ ^4I_{9/2},\ \mu=\tfrac{5}{2}\rightarrow F_1,\ ^2G_{1/2},\ \mu=\tfrac{1}{2}\ , \tag{2}$$

shown in Fig. 2 and found by Dieke[4] to occur at 19 430.93 cm^{-1}. The application of an external magnetic field $\mathbf{B}_0$ can shift by 1.26 cm^{-1} the wave number of the optical absorption (due to the transition shown in Fig. 2 from a Zeeman component of the Z_1 level to a component of the F_1 level) required to produce optical resonance with the laser emission. As the resonance is approached by scanning $|\mathbf{B}_0|$ at constant laser emission intensity, the intensity of the fluorescence from the transition,

$$E_1,\ ^4G_{7/2},\ \mu=\tfrac{3}{2}\rightarrow {}^4I_{11/2}\ \text{manifold} \tag{3}$$

shown in Fig. 2, increases due to increased pumping efficiency, and passes through a maximum at optical resonance. This statement is true for each fluorescence transition from E_1. The value of $|\mathbf{B}_0|$ for the resonance of the transition from the upper component of Z_1 to the lower component of F_1, and concomitant maximum of $E_1\rightarrow Y_1$ fluorescence intensity, is given by

$$|\mathbf{B}_0|_{\text{res}}=\frac{2\times 1.26\times hc}{|\mu_B|}({}^g g+{}^e g)^{-1}=(5.40\times 10^4\ \text{G})[({}^g g_\parallel^2\cos^2\theta+{}^g g_\perp^2\sin^2\theta)^{1/2}+({}^e g_\parallel^2\cos^2\theta+{}^e g_\perp^2\sin^2\theta)^{1/2}]^{-1}\ , \tag{4}$$

in which ${}^g g_\parallel$, ${}^g g_\perp$, ${}^e g_\parallel$, ${}^e g_\perp$ are the principal values of $\vec{g}$ for the ground Z_1 and excited F_1 states, respectively, and θ is the angle, $\cos^{-1}(\hat{\mathbf{B}}_0\cdot\hat{\mathbf{c}})$, between $\mathbf{B}_0$ and the c axis of the crystal. In Fig. 4 the experimental values measured during the course of the present work are plotted as circles for the case of the single-line fluorescence,

$$E_1,\ ^4G_{7/2},\ \mu=\tfrac{3}{2}\rightarrow Y_3,\ ^4I_{11/2},\ \mu=\tfrac{5}{2}\ . \tag{5}$$

(Y_3 at 2 026.90 cm^{-1} above Z_1 is the third crystal-field state of $^4I_{11/2}$.) The data were obtained for a $LaCl_3$ crystal containing 0.010 mole fraction $NdCl_3$ at ~ 1.6 K in a microwave cavity with no microwave field present. The solid line is a plot of Eq. (4) with the values of ${}^g g_\parallel$ and ${}^g g_\perp$ set equal to those given in Table I and with ${}^e g_\parallel$, ${}^e g_\perp$ and the F_1 term value adjusted to give a good fit to the circles: ${}^e g_\parallel=0.64$, ${}^e g_\perp=5.174$, F_1 term value of 19 431.03 cm^{-1}, F_1 term value minus the Ar^+ wave number equal to 1.36 cm^{-1}. These values give a root-mean-square deviation, 72 G, from the experimental data over the range of θ from 0 to $\pi/2$ and are to be compared with the values given in Table I. Values of the full width of the optical resonance at half maximum amplitude (measured during the course of the present work) are presented in Table II for $\cos^{-1}(\hat{\mathbf{B}}_0\cdot\hat{\mathbf{c}})=0.244\pi=44°$, and for various laser powers.

In our previous work we showed that there is a marked enhancement of the Nd^{3+} $E_1\rightarrow {}^4I_{11/2}$ fluorescence at those values of $|\mathbf{B}_0|$ for which there is EPR absorption by

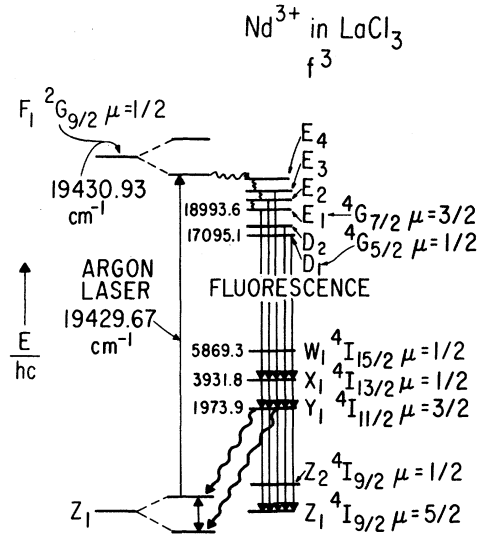

FIG. 3. Optical pumping cycles for Nd^{3+} in the $LaCl_3$ crystal. The numerical values are from Dieke (Ref. 4) and his symbolism is used.

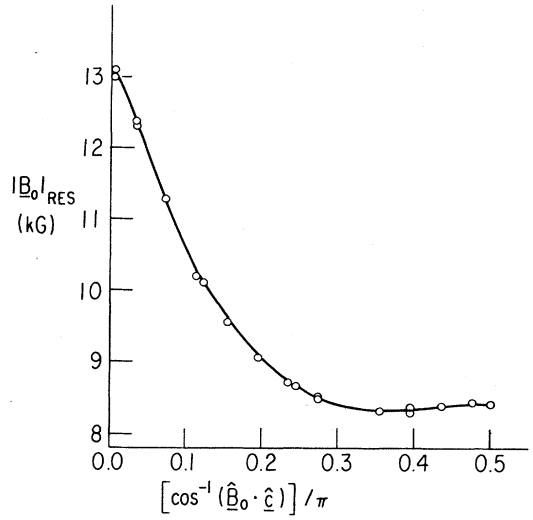

FIG. 4. Magnitude of field vs $[\cos^{-1}(\hat{\mathbf{B}}_0\cdot\hat{\mathbf{c}})]/\pi$ for optical resonance of the Ar^+ laser 19 429.67-cm^{-1} emission with the Nd^{3+} transition, Z_1, $^4I_{9/2}$, $\mu=\frac{5}{2}\rightarrow F_1$, $^2G_{9/2}$, $\mu=\frac{1}{2}$. The circles represent experimental data. The solid line is a plot of Eq. (4).

the Z_1 doublet when the following three experimental conditions are simultaneously established. (i) A $LaCl_3$ crystal with Nd^{3+} dilutely substituted at La^{3+} sites is irradiated with the 19 429.67-cm^{-1} Ar^+ laser emission while in direct contact with liquid He at ~ 1.6 K. (ii) A K-band microwave field is present in the microwave cavity in which the crystal is mounted. (iii) $|\mathbf{B}_0|$ is scanned in that range of values required for optical resonance of the laser emission with the transition from the higher-energy component of Z_1 to the lower component of F_1. This ODMR signal arises from the fact that resonant microwave irradiation of the ground Z_1 doublet increases the population of its upper component and does not affect the population of the lower component of F_1 whose g value is different. As a result the optical absorption intensity is increased, and this increased pumping rate enhances the fluorescence intensity. For values of $|\mathbf{B}_0|$ in the range for optical resonance with the transition from the lower Z_1 component to the lower component of the excited F_1 state (maximum fluorescence at $\sim 1.7\times 10^4$ G) the ODMR signal obtained with K_a-band microwaves is a deenhancement because in that case the lower component of Z_1 is depopulated by EPR absorption. A new mechanism for ODMR is observed and described in Secs. III and IV of this paper.

In the case of $LaCl_3$ crystals containing both Nd^{3+} and Er^{3+} dilutely substituted at La^{3+} sites, monitoring the $E_1\rightarrow {}^4I_{11/2}$ fluorescence of Nd^{3+} produces two ODMR signals under the experimental conditions described just above. One of these occurs at the value of $|\mathbf{B}_0|$ required for Nd^{3+} EPR and the other at the field for EPR of Er^{3+} in its ground crystal-field state. According to Dieke[4] and our own recent studies, Er^{3+} has no optical absorptions in the vicinity of the Ar^+ 19 429.67-cm^{-1} emission. Moreover, there are no excited states of Er^{3+} that lie above the ground $^4I_{15/2}$ state by amounts that are within

TABLE I. g values and lifetimes for Er^{3+} and Nd^{3+} dilutely substituted at La^{3+} sites in $LaCl_3$ (standard deviations are given in parentheses).

Species	Term	Dieke symbol	$g_\parallel$	$g_\perp$	Reference for g	Lifetime (s)	Reference for lifetime
Nd^{3+}	$^4I_{9/2}$, $\mu=\frac{5}{2}$	Z_1	3.99458(2)	1.76133(14)	13		
	$^4I_{11/2}$, $\mu=\frac{3}{2}$	Y_1	8.14[c]	0.00[c]	20	89×10^{-3}(21)	8
	$^4I_{13/2}$, $\mu=\frac{1}{2}$	X_1	10.1892(47)	1.3447	13	22.3×10^{-3}(1.6)	8
	$^4I_{15/2}$, $\mu=\frac{1}{2}$	W_1	9.548(21)	5.1212(11)	13	15.7×10^{-3}(1.1)	8
	$^4G_{5/2}$, $\mu=\frac{1}{2}$	D_1	1.34	0.72	5	28.2×10^{-6}(6)	6
	$^4G_{7/2}$ $\mu=\frac{3}{2}$	E_1	2.94	0.00	20	50×10^{-6}(1)	6
	$^2G_{9/2}$, $\mu=\frac{1}{2}$	F_1	0.64	5.01	5		
Er^{3+}	$^4I_{15/2}$, $\mu=\frac{5}{2}$		1.989(1)	8.757(2)	1		

20 cm^{-1} of the difference between either the $^4G_{7/2}$ or the $^2G_{9/2}$ state of Nd^{3+} and any other lower state of Nd^{3+}. Nevertheless, EPR of Er^{3+} in its ground state is signaled by an increase in Nd^{3+} fluorescence intensity. This is evidence for an interaction between Er^{3+} and Nd^{3+} that cannot occur by means of absorption by Er^{3+} of Nd^{3+} fluorescence or by a Foerster[22] radiationless exchange of energy between Er^{3+} and Nd^{3+} involving excited states. The nature of the interaction is revealed when the enhancement of Nd^{3+} $E_1 \rightarrow {}^4I_{11/2}$ fluorescence by Er^{3+} ground-state EPR is examined as a function of $\theta \equiv \cos^{-1}(\hat{\mathbf{B}}_0 \cdot \hat{\mathbf{c}})$. There are relatively sharp and pronounced increases in the intensity of the ODMR signal at those angles θ for which the ratio R of the ground doublet g value of Er^{3+} to the ground doublet g value of Nd^{3+} has any one of the values, $\frac{1}{2}$, 1, or 2. These conditions are expressed by the relation

$$\theta = \tan^{-1}\left[-\frac{R^2 {}^{Nd}g_{\parallel}^2 - {}^{Er}g_{\parallel}^2}{R^2 {}^{Nd}g_{\perp}^2 - {}^{Er}g_{\perp}^2}\right]^{1/2}, \tag{6}$$

in which $R \equiv {}^{Er}g/{}^{Nd}g = \frac{1}{2}$, 1, or 2 and the principal values are the values given in Table I. [There are numerous typographical errors in Eq. (3) of the paper by Furrer and Hutchison[21] that give an expression for θ as a function of R.] We have interpreted this result as demonstrating that the cross relaxation mentioned above occurs by means of exchange of ground doublet Zeeman quanta between Nd^{3+} and Er^{3+}. For the case, $R = n/m$, n Nd^{3+} quanta are exchanged for m Er^{3+} quanta with conservation of energy leading to a more rapid cross relaxation than for values of R that are not rational numbers. In previous experiments[17] in which Nd^{3+} fluorescence decay rates were measured for $LaCl_3$ crystals with cosubstituted Er^{3+}, enhanced rates of exchange of ground-state Zeeman quanta were observed for values of θ corresponding not only to the values of R, $\frac{1}{2}$, 1, and 2, but also to the values 3 and 4. Such increased rates have not been observed for $R = n/m$ with both n and m greater than 1. Four is the largest possible integral value of R for energy-conserving exchange and two is the largest possible value of m for $n = 1$.

Although there is no absorption of 19 429.67-cm^{-1} laser emission by Er^{3+} ions in $LaCl_3$,[4] we have observed recently that irradiation at this wave number of a crystal with Er^{3+} at 0.010 of the La^{3+} sites and Nd^{3+} at 0.010 of the sites, or of a crystal with only Er^{3+} at 0.010 of the sites, does produce a weak Er^{3+} fluorescence. This fluorescence is approximately 100 times less intense than that of a typical Nd^{3+} fluorescence for the crystals with equal numbers of Er^{3+} and Nd^{3+}. This may be due to Er^{3+} near structure defects, near trace impurities, or near another Er^{3+} as a result of a two-ion process. We do not believe this observation affects previous conclusions concerning cross relaxation.

TABLE II. Full width, $\Delta H_{1/2}$, at half maximum intensity of the optical resonance (fluorescence intensity vs $|\mathbf{B}_0|$ in the absence of microwave fields) as a function of laser power P and for $\cos^{-1}(\hat{\mathbf{B}}_0 \cdot \hat{\mathbf{c}}) = 0.244\pi = 44°$. Estimated uncertainty is given in parentheses.

P (mW)	$\Delta H_{1/2}$ (kG)	$\frac{\Delta H_{1/2}({}^{g}g + {}^{e}g)\lvert\mu_B\rvert}{2hc}$ (cm^{-1})
1539	5.22(2)	0.81
1083	3.48(2)	0.54
626	2.93(2)	0.46
184	1.45(2)	0.22

II. EXPERIMENTS

The procedures, techniques, and apparatus used were generally similar to those summarized in Sec. III C of the paper by Furrer and Hutchison.[21]

A. Crystal preparation and mounting

The $LaCl_3$ crystals used in the experiments were grown as described previously[23] from melts containing (a) 0.010 mole fraction $^{144}NdCl_3$ and 0.010 mole fraction $^{166}ErCl_3$; (b) 0.0010 mole fraction $^{144}NdCl_3$ and 0.0010 mole fraction $^{166}ErCl_3$; and (c) 0.010 mole fraction $^{144}NdCl_3$. The oxides used in the initial step of the presentation were La_2O_3, 0.999 999 mole fraction from Research Chemicals and Nd_2O_3, 0.97 fractional ^{144}Nd isotopic composition and Er_2O_3, 0.95 fractional ^{166}Er isotopic composition, from Oak Ridge National Laboratories. In the remainder of this paper we will refer to the crystals as containing 0.010 or 0.0010 mole fraction of the rare-earth trichloride, although we have composition information only on the melt from which they were grown and not on the crystals themselves.

Right circular cylinders 2.0 mm in diameter and 1.5 mm in altitude were machined with a lathe from pieces cleaved from the resulting boules. The plane ends of these cylinders were the cleavage planes and the c axis is known to be contained in these planes. The cylinder sidewalls were polished with cotton moistened with water-free toluene. They were washed with toluene and mounted inside fused silica tubes with 0.0505-cm wall thickness and length 2.0 cm. Apiezon grease was used in most cases to maintain the positions of the crystal cylinders in the tubes, whose inside circular cross section they nearly filled. The experimental results were unaffected qualitatively by the value of clearance between crystal and tube or the presence or absence of the grease. In some cases the tubes were sealed on their ends with fused silica caps by use of epoxy cement that was impervious to superfluid helium. The cleaving, machining, polishing, and encapsulating of the cylinders were all done in a nitrogen atmosphere in a dry box because of the hygroscopic character of $LaCl_3$. During the experiments the silica tubes containing the crystals were mounted with their axes parallel to the axis of the cylindrical microwave cavity, parallel to the microwave magnetic field and perpendicular to the $\mathbf{B}_0$ field. The incident laser beam was parallel to $\mathbf{B}_0$ as in previous work.[21] The sample tube was rotated about its axis while in direct contact with superfluid helium at ~ 1.5 to ~ 2.1 K. As a result of this arrangement, the angle θ between $\mathbf{B}_0$ and the c axis could be set at any desired value by means of a control external to the cryostat, and for all angles the optical path length of the laser beam in the crystal and the angle of incidence for the reflected laser beam were constant.

B. Optical methods

For these experiments the source of optical excitation was a Coherent Radiation cw Ar^+ laser. The 19 429.67 cm^{-1} (5 145.3 Å) emission line was employed. In multimode operation we used powers in the range from 0 to ~1900 mW measured at the exit of the laser with a calibrated power meter. The linewidth at half-height was ~10 GHz. In some experiments an oven-stabilized etalon produced a single longitudinal mode emission of 0–500 mW in a 60-MHz-wide line. For the same power levels there was no apparent difference between the results obtained in our experiments when using the two different laser configurations. We estimate that ~0.75 of the laser exit emission impinges on the $LaCl_3$ cylinders after passing through the Dewar windows and silica tubes.

The beam passed parallel to $\mathbf{B}_0$ through holes on the axes of the 30-cm-diam magnet poles, going through the encapsulated $LaCl_3$ cylinder mounted in the resonant cavity of the EPR spectrometer. For all values of $\theta \equiv \cos^{-1}(\hat{\mathbf{B}}_0 \cdot \hat{\mathbf{c}})$ (obtained as described in Sec. II A) the laser beam was normal to the polished circular surface of the $LaCl_3$ cylinder at its point of incidence on and exit from the crystal. After leaving the magnet the beam was focused onto the entrance slit of a Spex 1000 Czerny-Turner monochromator set to those fluorescence emission wavelengths that lay in the ranges, 585–595 and 660–670 nm. These emissions originated from the D, $^4G_{5/2}$ and E, $^4G_{7/2}$ manifolds[4] shown in Fig. 3.

The intensity of the fluorescence was monitored with an RCA 8572 photomultiplier cooled to ~270 K. In the ODMR experiments the signals from the photomultiplier were fed through an analog-to-digital converter to a multichannel analyzer and data averaging system, recorded and transferred to a minicomputer for further processing and storage.

C. Microwave EPR and ODMR methods

The reader is referred to the paper by Furrer and Hutchison[21] for descriptions of the K-band spectrometer, cryogenic equipment, EPR and ODMR signal detection and recording techniques, and methods of measurement of fluorescence and ODMR signal rise and fall times. The microwave frequencies during the present experiments were in the range 23.32–23.87 GHz. The output power of the klystron used was ~200 mW, approximately 0.25 of which was absorbed in the resonant cavity. The cavity Q with silica tube and crystal in place was ~3200. The cavity was a right circular cylinder with volume, 2.81 cm^3, operated in the TE_{011} mode.

D. Types of experiments

During the course of the work reported here the four types of experiments listed below were performed. Measurements were in most cases made with the $LaCl_3$ crystals at temperatures in the range from 1.6 to 2.2 K. The chemical composition of the crystals is given in Sec. II A. Crystals in sealed silica capsules and crystals in direct contact with superfluid helium were used in the various experiments.

Type 1. In the ranges of wavelengths from 585–595 nm and from 660–670 nm, which included the wavelengths of fluorescences originating from the D, $^4G_{5/2}$ and E, $^4G_{7/2}$ manifolds (see Fig. 3), all wavelengths of observed emissions were measured to a few tenths of a nm permitting their identification by comparison with Dieke's tables.[4]

Type 2. The intensities of fluorescence line emissions were measured as functions of laser power in the range from ~60 to ~1900 mW (measured at the laser exit) in the absence of both a static external magnetic field $\mathbf{B}_0$ and a microwave field. In the presence of $\mathbf{B}_0$, but with no microwave field present, they were measured as a function of $|\mathbf{B}_0|$ and of $\theta \equiv \cos^{-1}(\hat{\mathbf{B}}_0 \cdot \hat{\mathbf{c}})$.

Type 3. The effects of microwave EPR absorption by Nd^{3+} and Er^{3+} on the intensities of the individual fluorescences originating from the E_1, E_2, E_3, D_1, and D_2 (see Fig. 3) states were examined as a function of laser power and of $\theta \equiv \cos^{-1}(\hat{\mathbf{B}}_0 \cdot \hat{\mathbf{c}})$.

Type 4. The changes in the intensities of fluorescences with time after initiation of laser irradiation, after cessation of irradiation and after interruption of irradiation followed by continued irradiation, were measured as functions of laser power, of $\theta \equiv \cos^{-1}(\hat{\mathbf{B}}_0 \cdot \hat{\mathbf{c}})$ and of length of interruption.

III. RESULTS

A. Introduction

In the course of this work 28 different fluorescence line emissions of Nd^{3+} in $LaCl_3$ were investigated in experiments of the types described in Sec. II D. Our wavelength measurements for these emissions and also Dieke's values[4] used for identifications are listed in Table III. We categorize our reports of the results of these experiments according to (a) crystal compositions, (b) types of crystal mounting, and (c) ranges of laser pumping power. With respect to (a) there are three different compositions and for (b) two types of mounting; (a) and (b) are discussed in Sec. II A. With respect to (c), there was a limited range of laser powers over which temporal oscillations of fluorescence intensity occurred when the crystals were in sealed silica capsules.

We divide our descriptions of results on the basis of laser power into three parts: "low power" results, i.e., results obtained at powers lower than the range of power over which oscillations occurred; "intermediate power" results, i.e., results obtained for the power range in which oscillations occurred; and "high power" results, i.e., results for a range higher than the range of power over which oscillations occurred. These ranges varied with the temperature of the bath, the composition of the crystal, and the quality of the optically polished crystal surface. For crystals in sealed fused silica capsules containing 0.010 mole fraction $NdCl_3$ (whether or not 0.010 mole fraction of $ErCl_3$ is present in the crystal) and polished as described above, the "intermediate power" range is given in Table IV. For crystals containing 0.0010 mole fraction $NdCl_3$ and 0.0010 mole fraction $ErCl_3$ and polished as described above the lower and upper limits on the "intermediate power" range were considerably larger than for

the crystals that contained 0.010 mole fraction $NdCl_3$. The limits of the "intermediate power range" also varied with temperature. Over the range of T listed in Table IV the lowest laser pumping power at which oscillations occurred in the case of these crystals was ~ 15 mW and the highest was ~ 63 mW. For crystals of any composition in unsealed tubes or in direct contact with superfluid helium, oscillations were not observed for any value of laser power over the range from 0 to 1900 mW. One crystal cylinder used in the laser-beam interruption experiments mentioned in Sec. II D was polished in a somewhat different manner. In this case the laser powers required for oscillation were considerably higher than those given in Table IV, namely, 240–400 mW.

The values of laser pumping power given above and in Table III are values measured at the exit of the beam from the laser. As mentioned in Sec. II B approximately 0.75 of this power reached the surface of the crystal. Our measured value of absorptance due to the $^4I_{9/2} \rightarrow {}^2G_{9/2}$ transition (at room temperature) was ~ 0.5. The radiationless transitions to the $^4G_{7/2}$ manifold from the $^2G_{9/2}$ state and to the Z_1 state from higher energy states of the ^4I manifold dissipated ~ 0.25 of the excited-state energy.[4] Thus approximately 0.10 of the quoted laser power produced heating of the crystal and approximately 0.25 went into fluorescence emissions.

B. Results for crystals containing 0.010 mole fraction $NdCl_3$ (with and without 0.010 mole fraction $ErCl_3$ present) in sealed silica capsules in the absence of static and microwave magnetic fields

In the low power range only the 11 E_1 fluorescences of Nd^{3+} listed in Table II were observable with significant intensity. Some other lines with intensities ~ 0.010 of the E_1 lines were seen and identified as originating from the C_1 and D_1 states.[4] Typical fluorescence spectra recorded in the 5850–5950 and 6600–6700 Å ranges are shown in Fig. 5. (Although the spectra shown in this figure were obtained from unsealed crystals they are identical with those obtained in the low power range from crystals in sealed capsules.)

TABLE III. List of 28 fluorescence line emissions of Nd^{3+} in $LaCl_3$ single crystals investigated in this work.

Measured λ (Å) in air	Dieke λ (Å) in air	Upper state Dieke symbol[a]	Upper state E/hc (cm^{-1}) in vacuum	Lower state Dieke symbol[a]	Lower state E/hc (cm^{-1}) in vacuum
5875	5874	E_1	18 993.6	Y_1	1973.9
5887	5887	E_1	18 993.6	Y_2	2012.6
5893	5892	E_1	18 993.6	Y_3	2026.9
5899	5898	E_1	18 993.6	Y_4	2044.6
5902	5901	E_1	18 993.6	Y_5	2051.6
5904	5904	E_1	18 993.6	Y_6	2058.9
6657	6657	E_1	18 993.6	X_2	3974.9
6668	6667	E_1	18 993.6	X_3	3998.9
6674	6674	E_1	18 993.6	X_4	4012.9
6683	6682	E_1	18 993.6	X_5	4031.9
6687	6687	E_1	18 993.6	X_6	4042.1
5868	5868	E_2	19 012.9	Y_1	1973.9
5881	5881	E_2	19 012.9	Y_2	2012.6
6630	6629	E_2	19 012.9	X_1	3931.8
6659	6659	E_2	19 012.9	X_3	3998.9
6679	6679	E_2	19 012.9	X_4	4042.1
5871	5871	E_3	19 042.3	Y_2	2012.6
6646	6646	E_3	19 042.3	X_3	3998.9
6652	6652	E_3	19 042.3	X_4	4012.9
5859	5857	E_4	19 078.0	Y_2	2012.6
5848	5848	D_1	17 095.1	Z_1	0.00
5886	5886	D_1	17 095.1	Z_2	115.4
5934	5933	D_1	17 095.1	Z_4	244.4
6635	6635	D_1	17 095.1	Y_3	2026.9
6647	6646	D_1	17 095.1	Y_5	2051.6
6650	6649	D_1	17 095.1	Y_6	2058.9
6610	6610	D_2	17 098.9	Y_1	1973.9
6641	6641	D_2	17 098.9	Y_4	2044.2

[a]Reference 4.

TABLE IV. Ranges of laser power for oscillations of the intensity of the fluorescence from E_1, $^4G_{7/2}$, $\mu=\frac{3}{2}$; E_2, $^4G_{7/2}$, $\mu=\frac{5}{2}$; D_1, $^4G_{5/2}$, $\mu=\frac{1}{2}$; and D_2, $^4G_{5/2}$, for crystal containing 0.010 mole fraction $NdCl_3$ in sealed fused silica capsules, with or without $ErCl_3$ in the crystal.

Bath T (K)	$\cos^{-1}(\hat{\mathbf{B}}_0\cdot\hat{\mathbf{c}})$	Range of laser power for oscillation of fluorescence intensity (mW) Minimum	Maximum
1.50	$\pi/2$	41	63
1.65	$\pi/2$	33	49
1.65	0	33	49
1.80	$\pi/2$	30	46
2.10	$\pi/2$	15	25
2.10	0		25

In the intermediate power range the 17 fluorescence emissions, listed in Table II, due to transitions from the E_2, E_3, E_4, D_1, and D_2 states, were observed in addition to the E_1 transitions seen in the low power region. The intensities of all 28 of the Nd^{3+} fluorescences oscillated in synchrony at frequencies that depended on bath temperature and laser pumping power. Some typical plots of fluorescence intensity versus time are shown in Fig. 6 under conditions for which the frequency was approximately 0.5 Hz. Typically the frequency increased by the factor, approximately 1.3, as T increased from 1.5 to 2.1 K and increased by a factor approximately 2 as the power increased from the lowest to the highest value in the intermediate-power range. In the cases of the E_1 and D_1 emissions, as the laser power crossed the threshold into the intermediate power region, coming from the low power region the fluorescence intensity fell to a lower value and continued to oscillate between that lower value and the higher value characteristic of the low power regime. In the cases of the E_2, E_3, E_4, and D_2 emissions the fluorescence intensity increased as this threshold was crossed and continued to oscillate between this higher value and the lower low power value. The amplitudes of the oscillations at their onset are listed in Table V. The oscillatory behavior of the Nd^{3+} fluorescence was unaffected by the presence or absence of Er^{3+} in the crystal. When laser irradiation, at 1.8 K, of crystals containing 0.010 mole fraction $NdCl_3$ only, was interrupted (intensity reduced to zero) while the E_2, $^4G_{7/2}$, $\mu=\frac{5}{2}\rightarrow Y_1$, $^4I_{11/2}$, $\mu=\frac{3}{2}$ fluorescence was at the maximum of its intensity cycle, the $E_2\rightarrow Y_1$ intensity fell instantaneously to zero. When irradiation was resumed at the end of the "interruption time" a period elapsed before the fluorescence increased again to its initial value. The "recovery times," i.e., the elapsed times required for the fluorescence intensity to rise to ~ 0.10 of its full value after reinitiation of irradiation, are plotted versus the interruption times in the top two curves in Fig. 7. The times required for the intensity to increase from 0.10 to 0.90 of its fully recovered value were typically less than 0.5 s. The recovery time for given beam interruption time increased as the laser power was reduced. The recovery times were longer than the interruption times by factors ranging from ~ 10 for 1 s interruption to ~ 4 for 10 s interruption.

In the high power range the 28 fluorescence line emissions listed in Table III were observed. A typical fluorescence spectrum obtained in the high power range for the 5850–5950 and 6600–6700 Å ranges is presented in Fig. 8. When the $E_2\rightarrow Y_1$ fluorescence intensity was monitored during beam interruption experiments of the kind described above with laser power at 610 mW and the interruption times were <1.5 s the fluorescence ceased instantaneously upon beam interruption and reappeared instantaneously with full intensity upon reinitation of irradiation. For times between ~ 1.5 and ~ 8 s there was a short pulse of fluorescence, shown in Fig. 9, at the time irradiation was resumed. But as irradiation continued, after the pulse the intensity remained for a period of time at $\sim\frac{1}{20}$ of its initial value before the interruption before returning to its full initial value. The recovery times, i.e., the times from the initiation of the pulse of fluorescence until it rose to ~ 0.10 of full value were approximately equal to the interruption times. The times required for the fluorescence intensity to rise from ~ 0.10 to ~ 0.90 of full value at the end of the recovery time were in the range from 2.0 to 2.5 s. This behavior is shown in Fig. 9. The ratio of peak intensity of the pulse that occurred at the end of the interruption time to the full intensity is plotted versus interruption time in Fig. 10, for a laser power, 635 mW.

Figure 11 shows a typical behavior of fluorescence intensity as a function of laser pumping power as it increased in the range from 0 to ~ 400 mW after which the intensity increased only slightly.

Table II lists the full width at half maximum intensity of the optical resonance (fluorescence intensity versus $|\mathbf{B}_0|$ in the absence of microwave fields) as a function of laser power. Table VI lists ratios of fluorescence intensities for the E_1, E_2, D_1, and D_2 emissions as a function of laser power.

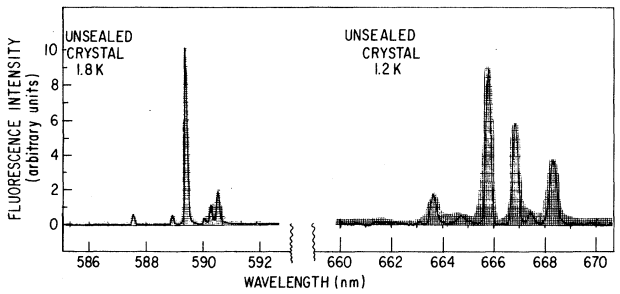

FIG. 5. Typical fluorescence spectra in the low power range for $LaCl_3$ crystals containing 0.010 mole fraction $NdCl_3$ $|\mathbf{B}_0|=0$.

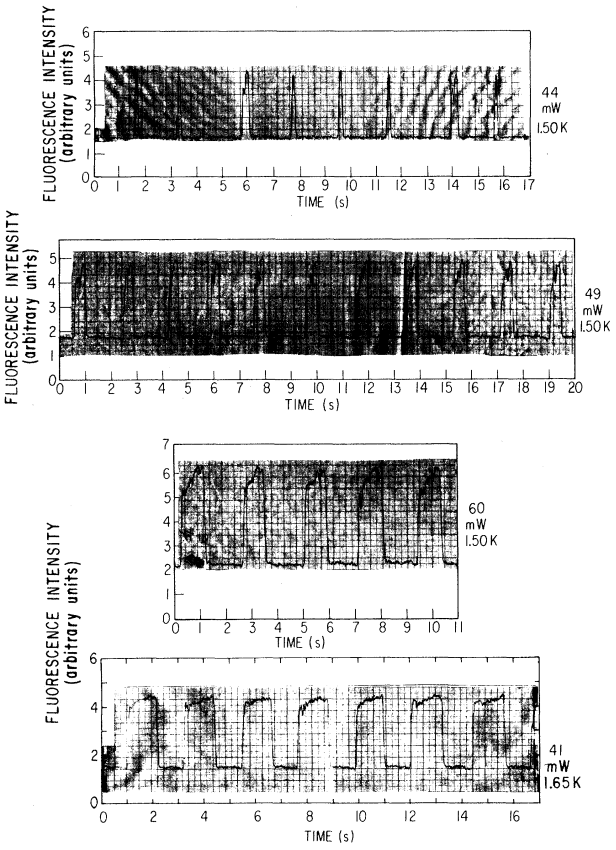

FIG. 6. Typical plots of fluorescence intensity vs time for $LaCl_3$ crystals containing 0.010 mole fraction $NdCl_3$ and placed in sealed fused silica capsules. The fluorescence emission is due to the transition, D_2, ${}^4G_{5/2} \rightarrow Y_1$, ${}^4I_{11/2}$, $\mu=\frac{3}{2}$. $|\mathbf{B}_0|=0$. Laser powers and bath temperatures are given for each plot.

C. Results for crystals containing 0.010 mole fraction $NdCl_3$ (with and without 0.010 mole fraction $ErCl_3$) in sealed silica capsules in the presence of static and microwave magnetic fields

In the lower power range our observations of optical resonance and ODMR signals of Nd^{3+} and Er^{3+} for each of the individual line emissions were the same as those made in previous work in our laboratory for the emission from the E_1, ${}^4G_{7/2}$, $\mu=\frac{3}{2}$ state to the Y, ${}^4I_{11/2}$ manifold,[16] and for the single transition, E_1, ${}^4G_{7/2}$, $\mu=\frac{3}{2} \rightarrow Y_3$, ${}^4I_{11/2}$, $\mu=\frac{5}{2}$.[17] Only one maximum of fluorescence intensity was observed for each of the 11 emissions as $|\mathbf{B}_0|$ was varied from 0 to 12 000 G in the absence of a microwave field, and the maximum showed the same behavior with $\theta \equiv \cos^{-1}(\hat{\mathbf{B}}_0 \cdot \hat{\mathbf{c}})$ as given by Eq. (4) above. ODMR signals for Nd^{3+} were obtained with all 11 fluorescences with the same θ behavior as for the previous studies.[20,21] For each of the fluorescences the Nd^{3+} ODMR signals were enhancements of their intensity. For several Nd^{3+} fluorescence emissions the intensities were enhanced by Er^{3+} EPR for values of $R \equiv {}^{Er}g/{}^{Nd}g = \frac{1}{2}, 1, 2, 3$ [see Eq. (6)]. For all emissions examined for this effect it was observed. The Nd^{3+} EPR enhancements of the fluorescences decayed exponentially upon termination of the microwave field while continuing laser irradiation. The bottom part of Fig. 12 shows typical temporal behavior of the ODMR enhancement on initiation and termination of the microwave field. In the equation,

$$I(t)=I_0 \exp[-(t-t_0)/\tau] , \tag{7}$$

TABLE V. Ratio of change of intensity at onset of oscillations to initial intensity as laser power is increased with $|\mathbf{B}_0|=0$.

Initial level of transition	Ratio
E_1 ${}^4G_{7/2}$ $\mu=\frac{3}{2}$	−0.10
E_2 ${}^4G_{7/2}$ $\mu=\frac{5}{2}$	+8.00
D_1 ${}^4G_{5/2}$ $\mu=\frac{1}{2}$	−0.30
D_2 ${}^4G_{5/2}$	+1.00

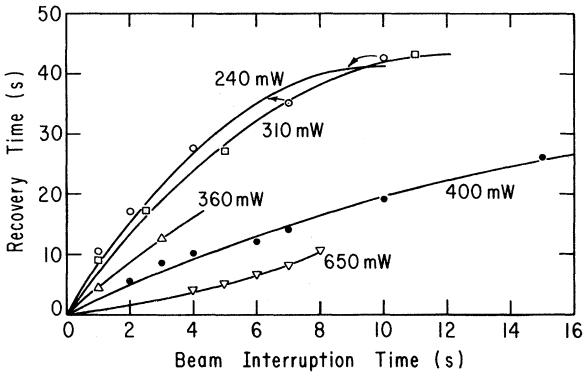

FIG. 7. Fluorescence recovery times (see text for definition) vs laser-beam interruption times, for $LaCl_3$ crystals at 1.8 K containing 0.010 mole fraction $NdCl_3$. The fluorescence emission is due to the transition, E_2, ${}^4G_{7/2}$, $\mu=\frac{5}{2} \rightarrow Y_1$, ${}^4I_{11/2}$, $\mu=\frac{3}{2}$. For each curve the corresponding laser power is listed.

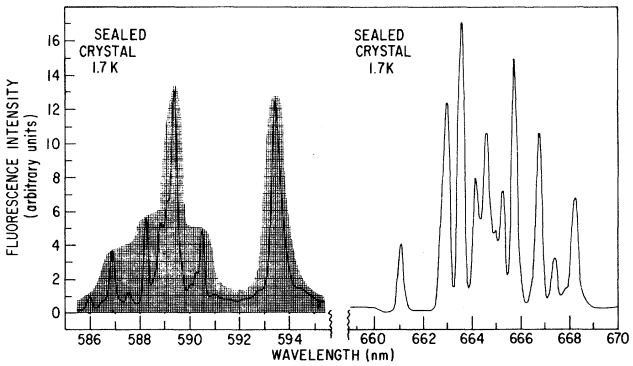

FIG. 8. Typical fluorescence spectra in the high power range for $LaCl_3$ crystals containing 0.010 mole fraction $NdCl_3$. $|\mathbf{B}_0|=0$.

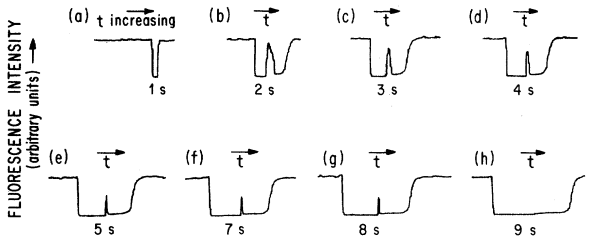

FIG. 9. Fluorescence intensity vs time during beam interruption experiments for a $LaCl_3$ crystal at 1.8 K containing 0.010 mole fraction NdCl and with laser power, 625 mW. $|\mathbf{B}_0|=0$. The fluorescence emission is due to the Nd^{3+} transition, E_2, ${}^4G_{7/2}, \mu=\frac{5}{2} \rightarrow Y_1$, ${}^4I_{11/2}, \mu=\frac{3}{2}$.

in which I_0 is the initial steady-state fluorescence enhancement by Nd^{3+} EPR at time t_0 and t is the time at which the microwave field was terminated, the value of τ was adjusted to give a least-squares fit to decay curves such as those shown in Fig. 12 for the $E_1 \rightarrow Y_3$ emission. For values of $R \equiv {}^{Er}g/{}^{Nd}g \neq \frac{1}{2}, 1, 2, 3$ [see Eq. (6)] the exponential relation, (7), gave a good fit to the data. At or near values of θ for which $R=\frac{1}{2}$, 1, 2, or 3 the Nd^{3+} decays deviated appreciably from the exponential form. As previously reported by Furrer and Hutchison[21] the $1/e$ times for the decays were markedly depressed below their values at nearby field angles. At 1.64 K τ had the value, 43 ms for 18 mW laser power and decreased to approximately 30 ms as power increased and the intermediate power range was approached.

The presentation of the experimental results for the intermediate range of laser power in which oscillations of the fluorescence intensity occurred is facilitated by first discussing the high power region. Because various of the behaviors of these systems in the intermediate range were in a certain sense an oscillation between the low power

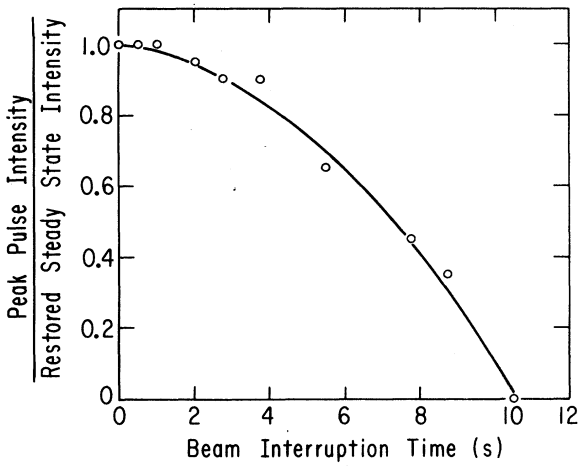

FIG. 10. Ratio of peak intensity of fluorescence pulse to fully recovered intensity for beam interruption experiments for a $LaCl_3$ crystal at 1.8 K containing 0.010 mole fraction $NdCl_3$ and with laser power, 625 mW. $|\mathbf{B}_0|=0$. The fluorescence emission is due to the transition, E_2, ${}^4G_{7/2}, \mu=\frac{5}{2} \rightarrow Y_1$, ${}^4I_{11/2}, \mu=\frac{3}{2}$.

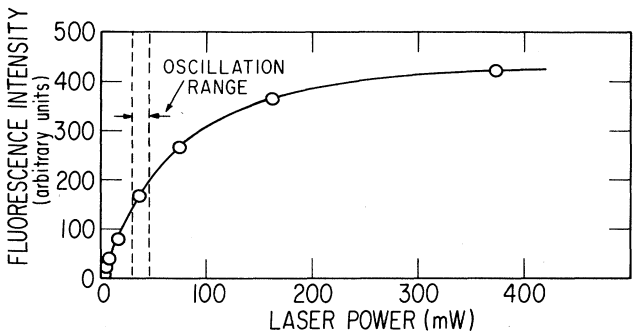

FIG. 11. Fluorescence intensity vs laser power for $LaCl_3$ crystals in sealed fused silica capsules at 1.8 K and containing 0.010 mole fraction $NdCl_3$. The fluorescence is due to the transition, E_1, ${}^4G_{7/2}, \mu=\frac{3}{2} \rightarrow Y_3$, ${}^4I_{11/2}, \mu=\frac{5}{2}$. The angle between $\mathbf{B}_0$ and the c axis is $\sim\pi/4$. $|\mathbf{B}_0|=0$.

and the high power behaviors, knowledge of the high power behaviors thus aids in interpreting the intermediate power behavior. In the high power range the 20 line emissions from E states (11 from E_1, 6 from E_2 and 3 from E_3, see Table III) showed only one optical resonance maximum in intensity versus $|\mathbf{B}_0|$ in the absence of EPR, for all values of $\theta \equiv \cos^{-1}(\hat{\mathbf{B}}_0 \cdot \hat{\mathbf{c}})$. Typical single maxima are shown for E_1 and E_2 emissions in Figs. 13 and 14. The eight D_1 and D_2 emissions showed from 1 to 4 maxima of intensity as $|\mathbf{B}_0|$ was scanned. Typical multiple maxima are shown for two different D_1 emissions in Fig. 14. These are plots of measurements in the presence of a microwave field; in the absence of the microwave field the plots are, except for the absence of the ODMR signals, the same as those shown in Figs. 13 and 14. In the high power range both Nd^{3+} and Er^{3+} EPR produced deenhancements of the intensity of all fluorescences from the E_1 state at those same fields for which in the low power range they produced enhancements, for all values of $\theta \equiv \cos^{-1}(\hat{\mathbf{B}}_0 \cdot \hat{\mathbf{c}})$ for which EPR is observed and for all laser powers up to $\sim$1000 mW. This is shown for two different E_1 emissions in Fig. 14. The intensity decrease caused by Nd^{3+} or Er^{3+} EPR was $\sim$0.10 of the maximum optical resonance intensity. As power increased above 1000 mW the ODMR signals were not ob-

TABLE VI. Ratios of fluorescence intensity vs laser power.

Laser power (mW)	I_{E_2}/I_{E_1}	$(I_{D_2}+I_{D_3})/I_{D_1}$
86	0.0267	0.065
122	0.0276	0.066
135	0.0469	0.079
192	0.0820	0.103
260	0.428	0.182
303	0.938	0.198
373	1.83	0.257
525	2.58	0.341

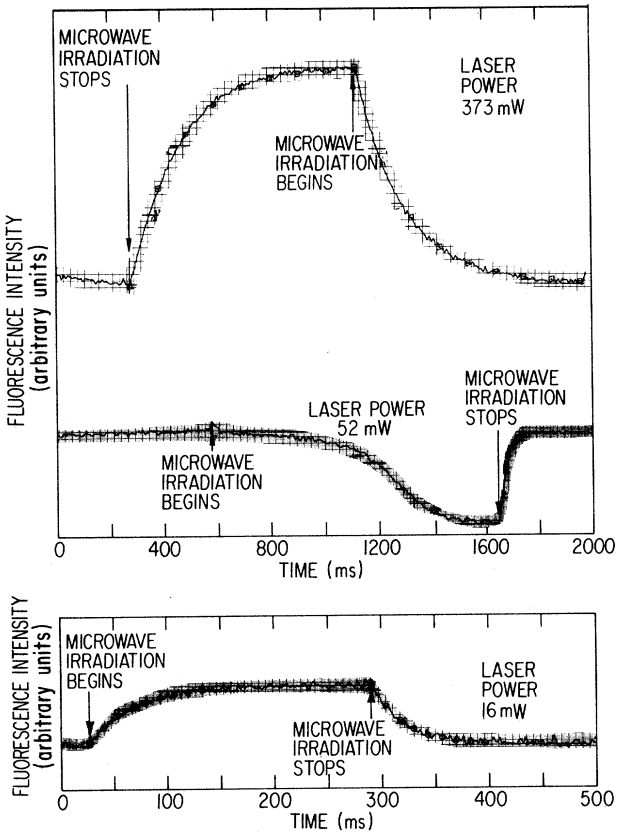

FIG. 12. Typical temporal behavior of Nd^{3+} EPR enhancement of fluorescence intensity on initiation and termination of the K-band microwave field, for crystals of $LaCl_3$ at 1.62 K containing 0.010 mole fraction $NdCl_3$ and placed in fused silica capsules. The fluorescence is due to the transition, E_1, $^4G_{7/2}$, $\mu=\frac{3}{2}\rightarrow Y_3$, $^4I_{11/2}$, $\mu=\frac{5}{2}$. For each curve the corresponding laser power is given. The angle between $\mathbf{B}_0$ and the c axis is $\sim\pi/4$.

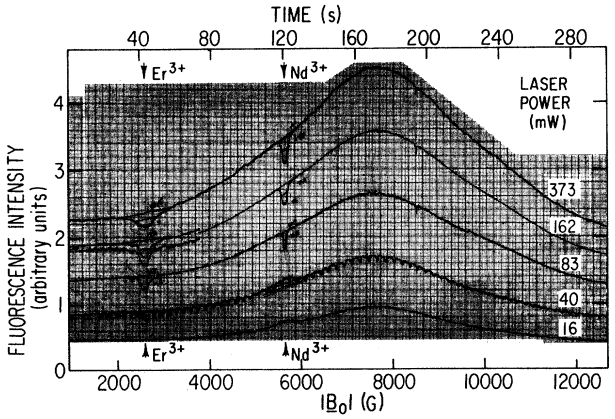

FIG. 13. Typical chart recordings of fluorescence intensity vs $|\mathbf{B}_0|$ for $LaCl_3$ crystals at 1.8 K containing 0.010 mole fraction $NdCl_3$ and 0.010 mole fraction $ErCl_3$ and placed in sealed fused silica capsules. A K-band microwave field is present. The fluorescence emission is due to the transition, E_1, $^4G_{7/2}$, $\mu=\frac{3}{2}\rightarrow Y_3$, $^4I_{11/2}$, $\mu=\frac{5}{2}$. For each curve the corresponding laser power is given. The angle between $\mathbf{B}_0$ and the c axis is $\sim\pi/4$.

served. Both Nd^{3+} and Er^{3+} EPR caused E_2 emission intensities to increase as shown for one emission in Fig. 14. E_2 ODMR signals were observed for all values of $\theta=\cos^{-1}(\hat{\mathbf{B}}_0\cdot\hat{\mathbf{c}})$ and for laser powers up to $\sim$1000 mW. They were not observed above that power. Under most conditions D_1 and D_2 emissions gave ODMR signals for both Nd^{3+} and Er^{3+} that were enhancements of fluorescence intensity. Such enhancements are shown in Fig. 14. An exception is the case of D_1 emissions which showed Nd^{3+} and Er^{3+} EPR deenhancements just above and up to $\sim$10 mW above the oscillation range and then gave enhancement signals at higher laser powers. This behavior is shown in Fig. 15. The same figure also shows the structure that appeared in the Er^{3+} ODMR signal just above the intermediate power range. For E_2, D_1, and D_2 emissions we observed new ODMR signals not seen in the low power range. These are apparent in the plot for the $D_2\rightarrow Y_4$ emission in Fig. 14. We have positively identified them, from their behavior as $\theta=\cos^{-1}(\hat{\mathbf{B}}_0\cdot\hat{\mathbf{c}})$ is varied, as ODMR signals from the nearest and next-nearest Nd^{3+} ground-state pairs. The

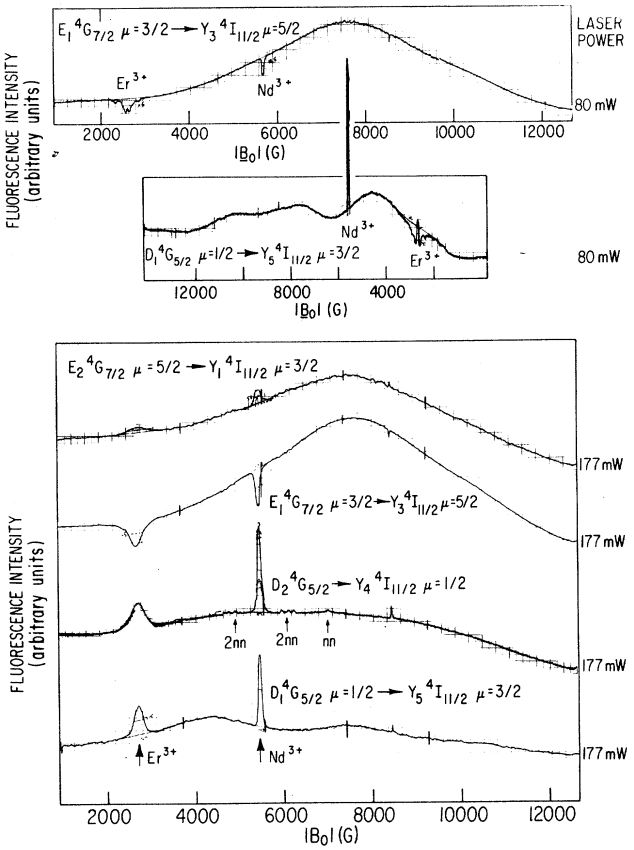

FIG. 14. Typical chart recordings of fluorescence intensity vs $|\mathbf{B}_0|$ for $LaCl_3$ crystals at 1.8 K containing 0.010 mole fraction $NdCl_3$ and 0.010 mole fraction $ErCl_3$ and placed in sealed fused silica capsules. A K-band microwave field is present. For each curve the corresponding transition producing the fluorescence and the laser power are given. The angle between $\mathbf{B}_0$ and the c axis is $\sim\pi/4$.

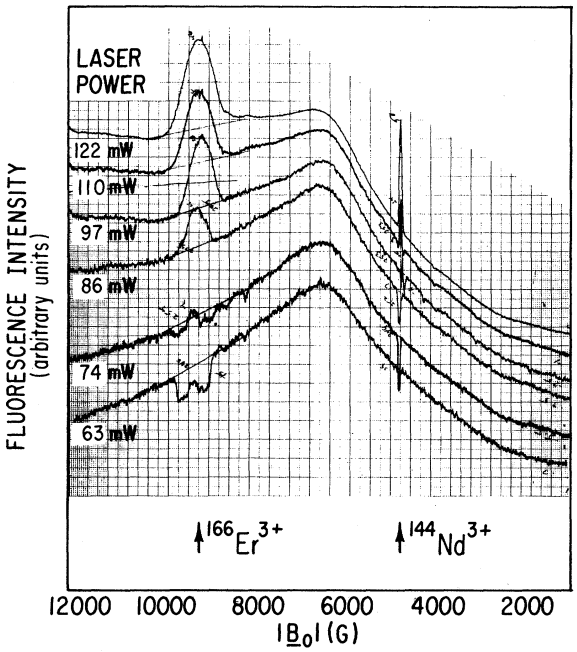

FIG. 15. Typical chart recording of fluorescence intensity vs $|\mathbf{B}_0|$ for a $LaCl_3$ crystal at 1.62 K containing 0.010 mole fraction $NdCl_3$ and 0.010 mole fraction $ErCl_3$ and placed in a sealed fused silica capsule. A K-band microwave field is present. The fluorescence is due to the transition, D_1, ${}^4G_{5/2}$, $\mu=\frac{1}{2}\rightarrow Z_4$, ${}^4I_{9/2}$, $\mu=\frac{1}{2}$. For each curve the corresponding laser power is given. The angle between $\mathbf{B}_0$ and the c axis is ~ 0.

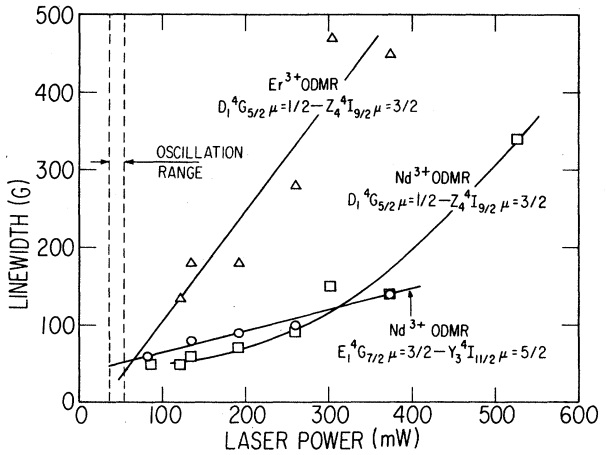

FIG. 16. ODMR linewidths vs laser power for $LaCl_3$ crystals at 1.6 K containing 0.010 mole fraction $NdCl_3$ and 0.010 mole fraction $ErCl_3$ and placed in sealed fused silica capsules. For each curve the corresponding transition producing the fluorescence is given. A K-band microwave field is present. The angle between $\mathbf{B}_0$ and the c axis is $\sim\pi/4$. The solid lines passing through the triangles and circles are straight lines least-squares fitted to the data. The line through the squares is a parabola least-squares fitted to the data.

splitting of the $2n$ ODMR signal into a triplet in this spectrum confirms that the plane ends of this crystal sample cylinder contained the a axis. The nn and $2n$ ODMR signals were observable only for attenuator settings corresponding to microwave powers greater than 100 mW directed toward the cavity assembly.

The intensities and linewidths of the ODMR signals in the high power range showed a strong dependence on laser power. Figure 11 shows the change in intensity with power for one transition. The power dependence of linewidth is shown for three cases in Fig. 16. In all cases the ODMR linewidth increased as laser power was increased and as $\theta\equiv\cos^{-1}(\hat{\mathbf{B}}_0\cdot\hat{\mathbf{c}})$ was varied such that the ODMR line shifted to higher magnetic fields. At laser powers $<\sim 30$ mW above the oscillation range Er^{3+} and in some cases Nd^{3+} ODMR lines showed fine structures with up to five maxima. The decays of the Nd^{3+} and Er^{3+} EPR enhancements or deenhancements of fluorescence showed single exponential decays for all values of $\theta\equiv\cos^{-1}(\hat{\mathbf{B}}_0\cdot\hat{\mathbf{c}})$ with standard deviations in τ [Eq. (7)] that were less than $0.04|\tau|$. The temporal behavior of fluorescence intensity from the $E_1\rightarrow Y_3$ transition on initiation and termination of microwave radiation at the Nd^{3+} EPR frequency, with continued laser irradiation, is shown at the top of Fig. 12. In contrast to the results obtained in the low-power range, τ increases with increase in laser power. This behavior is shown in Fig. 17 for one fluorescence. For values of $R\equiv{}^{\mathrm{Er}}g/{}^{\mathrm{Ng}}g\neq\frac{1}{2}$, 1, 2, or 3 there was no change from the exponential decay behavior or in the value of τ, in striking contrast with the behavior in the low power region as described above.

In the "intermediate power" range as $|\mathbf{B}_0|$ was scanned from 0 to 12 000 G the optical resonance gave only one maximum of fluorescence intensity for E emission and from one to four maxima for D emissions, just as described above for the high power region. Figure 18 shows this behavior for one E_1 emission and a D_1 and a

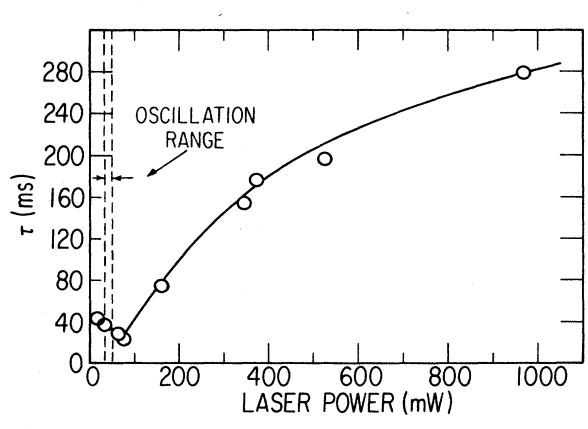

FIG. 17. Value of τ in Eq. (7) for ODMR signal intensity vs time, as a function of laser power for K-band microwave field termination experiments with $LaCl_3$ crystals at 1.64 K containing 0.010 mole fraction $NdCl_3$ and 0.010 mole fraction $ErCl_3$ and placed in sealed fused silica capsules. $\cos^{-1}(\hat{\mathbf{B}}_0\cdot\hat{\mathbf{c}})=\sim\pi/4$. The fluorescence is due to the transition, E_1, ${}^4G_{7/2}$, $\mu=\frac{3}{2}\rightarrow Y_3$, ${}^4I_{11/2}$, $\mu=\frac{5}{2}$.

D_2 emission, with superposed temporal oscillations.

In the intermediate power range intiating a microwave field during fluorescence intensity oscillations and in the presence of an external static field with the value of $|\mathbf{B}_0|$ required for Nd^{3+} EPR generated an ODMR signal that for E_1 emissions oscillated between the enhancement shown in the low power region and the deenhancement shown in the high power region. In other words, the ODMR signal oscillated at the fluorescence oscillation frequency between the types of signals observed in the low power and high power ranges described above. The application of a microwave field produced a very different effect in the case of Er^{3+} EPR with laser pumping power in the intermediate power range. For E_1 and D_1 fluorescences if the fluorescence intensity was at its high value for the oscillation cycle when the EPR condition was established by the initiation of a microwave field, then the oscillation continued for the next $\frac{1}{2}$ cycle at which time it reached its low value and remained there; the oscillation ceased and did not reappear as long as the conditions for Er^{3+} EPR were maintained. The cessation of oscillation occurred only when the microwave power was greater than 100 mW. On the other hand, if the fluorescence intensity was at its low value of the cycle when the EPR condition for Er^{3+} was established, then the intensity remained at its low value and the oscillation did not reappear until the microwave field was terminated. For D_2, E_2, and E_3 fluorescences the behavior is the opposite of that for the E_1 and D_1 cases. For D_2, E_2, and E_3 if the fluorescence intensity was at its high value of the cycle when microwave irradiation was initiated with $|\mathbf{B}_0|$ at the value required for Er^{3+} EPR then the intensity remained at that value and oscillation ceased and did not appear again until the microwaves were terminated. However, if the intensity was at its low value when the microwave field was initiated, the oscillation continued for $\frac{1}{2}$ cycle at which time it reached its high value and oscillation ceased and did not reappear until the microwave field was removed. These behaviors are illustrated in Fig. 19. The locking of the previously oscillating D_1 fluorescence intensity into its low-intensity value as $|\mathbf{B}_0|$ was scanned through the value for Er^{3+} EPR and the locking of a D_2 fluorescence into its high-intensity value are shown in Fig. 15. Note that the effect on the oscillating fluorescence of initiating EPR absorption of microwave radiation was to quench the oscillation and push the intensity to that value, enhanced or deenhanced, which characterized the ODMR signal in the high power range.

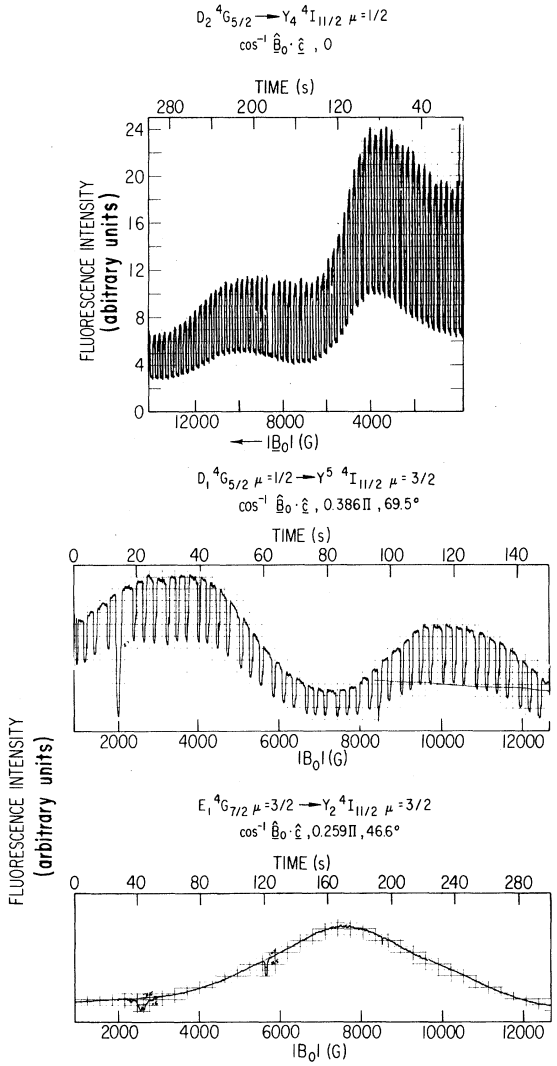

FIG. 18. Typical chart recordings of fluorescence intensity vs time and $|\mathbf{B}_0|$ for crystals of $LaCl_3$ at 1.8 K containing 0.010 mole fraction $NdCl_3$ and 0.010 mole fraction $ErCl_3$ and placed in sealed fused silica capsules. A K-band microwave field is present. For each recording the corresponding fluorescence transition and value of $\cos^{-1}(\hat{\mathbf{B}}_0\cdot\hat{\mathbf{c}})$ are given. Microwave frequency in range, 23.32–23.87 GHz.

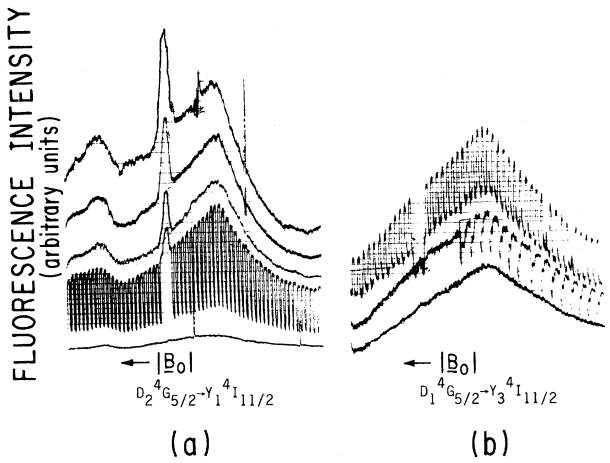

FIG. 19. (a) and (b) Typical behaviors of fluorescence intensity oscillations as $|\mathbf{B}_0|$ is scanned through the value for EPR in the presence of a K-band microwave field. Behavior for $LaCl_3$ crystals at 1.8 K containing 0.010 mole fraction $NdCl_3$ and 0.010 mole fraction $ErCl_3$ and placed in sealed fused silica capsules. For each curve is given the corresponding fluorescence transition.

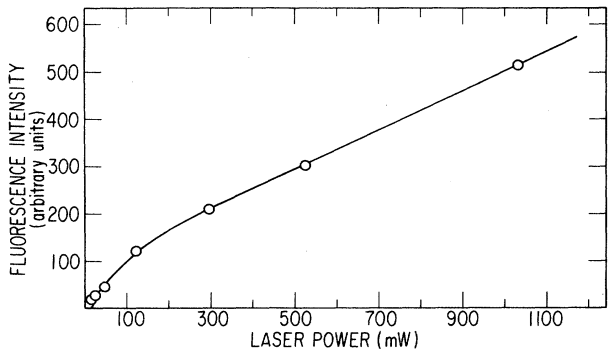

FIG. 20. Fluorescence intensity vs laser power for $LaCl_3$ crystals in unsealed fused silica capsules at 1.8 K and containing 0.010 mole fraction $NdCl_3$ and 0.010 mole fraction $ErCl_3$. The fluorescence is due to the transition, E_1, ${}^4G_{7/2}$, $\mu=\frac{3}{2}\rightarrow Y_3$, ${}^4I_{11/2}$, $\mu=\frac{5}{2}$. The laser beam is parallel to the c axis.

D. Results for crystals containing 0.0010 mole fraction $NdCl_3$ and 0.0010 mole fraction $ErCl_3$ in sealed silica capsules

The results for these crystals were, with the following exceptions, the same as those described in Secs. III B and III C for crystals in sealed capsules containing the higher concentrations of $NdCl_3$ and $ErCl_3$. (a) The intermediate power range extended from 335 to 460 mW, i.e., these were the lowest and highest laser pumping powers for which oscillations of fluorescence intensity were observed under any conditions. (b) No fluorescences from the D manifold were ever observed. (c) There was no effect of Nd^{3+} or Er^{3+} EPR on the nature of the oscillations.

E. Results for crystals in unsealed silica capsules

The results for crystals in unsealed fused silica tubes were, for all laser powers, i.e., 0 to $\sim$1900 mW, similar to those for crystals in sealed capsules in the low power range. Oscillations of fluorescence intensity were never observed and only the E_1 fluorescences were found. Figure 20 shows the behavior of fluorescence intensity as a function of laser power for the E_1, ${}^4G_{7/2}$, $\mu=\frac{3}{2}\rightarrow Y_3$, ${}^4I_{11/2}$, $\mu=\frac{5}{2}$ transition.

IV. DISCUSSION AND INTERPRETATION OF RESULTS

A. Introduction

In Secs. III B, III C, and III D, we noted in detail the striking differences between the results obtained (a) when the laser power was less than that of the range in which oscillations occurred (i.e., in the low power range defined above) and (b) when it was above that range (i.e., in the high power range). These differences in the fluorescence and ODMR results are summarized concisely in Table VII. This summary clearly indicates that the mechanisms for generation of the fluorescences and of the ODMR signals at the higher laser powers must be very different from those mechanisms discussed in Sec. I that are adequate for understanding the low power observations. The essential fact for understanding the main features of these differences is that heating of the crystal environment of the rare-earth ions, through phonon generation by radiationless transitions of the types depicted by wavy lines in Figs. 2 and 3, results in appreciably higher temperatures of the crystal in the higher power region. Under these conditions a new type of ODMR response is observed, the mechanism for which is based on phonon heating produced by spin-lattice relaxation following microwave absorption. The fluorescence intensity changes that accompany the phonon heating result from the effect of the crystal temperature rise on the population of the emitting states. The evidence for these temperature changes comes from four sources: (a) the change in width of the optical resonance with change in laser power; (b) the variations in the ratios of intensities of different fluorescence emissions with varying laser power; (c) the marked changes in ODMR linewidths as a function of laser power; and (d) the measured values of the thermal properties of $LaCl_3$ crystals and of the silica with which the crystals were encapsulated. In Appendix A we discuss in detail the information concerning crystal temperature that can be obtained from these sources. Sources (a), (b), and (d) show clearly that laser irradiation raises markedly the temperature of the crystal but they do not provide quantitative values of the temperature. Source (c) provides us with a crude estimate of the temperature. We estimate that at the upper limit of the oscillation range the crystal temperature is $\sim$25 K and at laser power, 500 mW, is $\sim$35 K.

In Sec. II A, we have described in detail the experimental arrangement that we devised in order that (a) the very hygroscopic crystal could be handled in the laboratory atmosphere, (b) the angle θ between $\mathbf{B}_0$ and the c axis could be set at any desired value, and (c) the optical pathlength in the crystal and angle and intensity of laser-beam reflection from the crystal would be constant for all values of θ. Our considerations described in Appendix A 4 show that the silica capsule played an important role in determining crystal temperature during laser irradiation. As stated in Sec. III E, for crystals not in sealed silica capsules the results for all laser powers were similar to those in the second column of Table VII and not those of the third column, confirming the role of the capsule in determining temperature. The capsule was mandatory for most of our experiments because of the necessity of meeting conditions (a), (b), and (c) described above.

In Table I we have summarized, in the seventh and eighth columns, information concerning lifetimes of the states that play a role in our experiments. In view of the fact that, as already pointed out, these lifetimes, of order 30 to 50 μs, are relatively long compared with the thermal equilibration times, of order 1 μs, the evidences of increase of crystal temperature with laser power presented in Appendix A may be expected to indicate that the populations of E_1, E_2, E_3, and E_4 levels approach Boltzmann distributions characteristic of the temperatures crudely estimated for the crystal. The same statement may of course be made for the D_1, D_2, and D_3 levels and also for the two Zeeman levels of the ground state. At $\sim$25 K, the estimated temperature at the upper oscillation limit, the difference in populations of the two

Zeeman components of the ground Z_1 state (the microwave frequency was 2.35×10^{10} Hz) would be only 0.02 of their total population, to be compared with 0.49 of the total at 1.6 K. The fraction of the E_1 plus E_2 population in the E_2 state would rise at 25 K to 0.31 from the value, 0.00, at 1.6 K, with a corresponding drop in the E_1 fraction from 1.00 to 0.69. The fraction of the D_1 plus D_2 population found in the D_2 state would be 0.45 compared with 0.03 at 1.6 K. Even the Z_2 level at 115.39 cm^{-1} above Z_1 would contain 0.0013 of the Z manifold population at 25 K and 0.01 at 35 K.

B. Effects of the increase of crystal temperature

1. Fluorescence intensities

The nine new E fluorescences observed above the oscillation range (see Table VII, first row) result from the increased populations, described in Sec. IV A, of the higher energy levels of the E manifolds. The eight observed D emissions found only for powers above the oscillation range are accounted for by an indirect mechanism for populating the D_1 and D_2 states that becomes possible at higher temperatures. Comparison of wave numbers of possible Nd^{3+} $E_1,E_2,E_3\rightarrow X,Y$ transitions and possible $Z_2\rightarrow D_1,D_2$ absorptions, based on Dieke's[4] tables (see also Table III and Fig. 4), reveals that there are 11 agreements (within 4 cm^{-1}) of emission and absorption. Because of the thermal populating of the Z_2 level at higher laser powers (see Sec. V C), energy of $E_1,E_2,E_3\rightarrow X,Y$ transitions can excite $Z_2\rightarrow D_1,D_2$ transitions through Foerster[22] energy transfer, thereby populating D_1 and D_2 levels. For this reason the additional eight D fluorescences (see Table VII, first row) are observed at the higher laser powers. It is also to be noted that as reported in Sec. III D, no D fluorescences were observed at higher laser powers in crystals for which the Nd^{3+} concentration was 10 times lower than that for which D emission was observed. This fact is in agreement with expectations for the proposed populating mechanisms because of the strong interionic distance dependence of the energy exchange processes that are involved.

2. ODMR

Comparison of the second and third columns of Table VII reveals the very different characters of the ODMR signals in the low power and high power ranges. Most noticeable is the fact that, whereas in the low power range the E_1 signals are enhancements of intensity, in the

TABLE VII. Summary of fluorescence and ODMR results obtained for $LaCl_3$ crystals with Nd^{3+} and Er^{3+} dilutely substituted at La^{3+} sites.

	Laser power	
	Low power range	High power range
Nd^{3+} fluorescences with appreciable intensity	11 transitions $E_1,\ {}^4G_{7/2}\rightarrow \begin{Bmatrix} X,\ {}^4I_{13/2} \\ Y,\ {}^4I_{11/2} \end{Bmatrix}$	Same 11 plus 9 from E_2, E_3, E_4 and 8 from D_1, D_2.
Optical resonance fluorescence intensity versus $\lvert\mathbf{B}_0\rvert$	1 maximum only for resonance of $(F_1,\ {}^2G_{3/2}\leftrightarrow Z_1,\ {}^4I_{9/2})$ with Ar^+ 19429.67 cm^{-1} emission.	20 E transitions have 1 maximum only for resonance of $(F_1,\ {}^2G_{3/2}\leftrightarrow Z_1,\ {}^4I_{9/2})$ with Ar^+ 19429.67 cm^{-1} emission. 8 D_1, D_2 transitions have 1 to 4 maxima.
ODMR	For all 11 transitions and all values of $\hat{\mathbf{B}}_0\cdot\hat{\mathbf{c}}$	All values of $\hat{\mathbf{B}}_0\cdot\hat{\mathbf{c}}$ E_1 transitions give deenhancements.
	Nd^{3+} gives enhancement and Er^{3+} (for $R=\frac{1}{2},1,2,3,4$) gives enhancement.	E_2, D_1, D_2 transitions give enhancements.
ODMR signal decay	For $R\equiv {}^{Er}g/{}^{Nd}g\neq\frac{1}{2},1,2,3,4$, single exponential decay. For $R\equiv {}^{Er}g/{}^{Nd}g=\frac{1}{2},1,2,3,4$, not exponential decay.	All angles, including ${}^{Er}g/{}^{Nd}g=\frac{1}{2},1,2,3,4$, single exponential decay.
$I(t)=I(t_0)e^{-(t-t_0)/\tau}$	τ decreases as laser power increases. Near ${}^{Er}g/{}^{Nd}g=\frac{1}{2},1,2,3,4$, $1/e$ time decreases. For ${}^{Er}g/{}^{Nd}g=\frac{1}{2},1,2,3,4$, $1/e$ time dependent on $\hat{\mathbf{B}}_0\cdot\hat{\mathbf{c}}$.	τ increases as laser power increases. $1/e$ time is constant, for all $\hat{\mathbf{B}}_0\cdot\hat{\mathbf{c}}$.
ODMR linewidth	No change with laser power over most of range.	Increases with increase in laser power.

high power range they are deenhancements. The mechanism discussed in Sec. I for the production of ODMR signals in the low power range depends on the fact that microwave absorption appreciably alters the populations of the two Zeeman components of the ground Z_1 state. We have pointed out in Sec. IV A that at the crystal temperatures attained for laser powers above the oscillation threshold, the difference in populations of these two components in the absence of microwave absorption is 0.02 or less of their total population, compared with 0.49 at 1.6 K. Therefore the microwave absorption due to magnetic resonance at higher laser powers cannot produce appreciable alteration of the population and the low temperature mechanism for production of ODMR becomes ineffective.

Appendix B gives a calculation of the microwave power absorbed by the crystal when the conditions for EPR of Nd^{3+} or Er^{3+} are realized. It is shown there that EPR results in the dissipation of ~ 7 and ~ 10 mW of microwave power as heat at 25 and 35 K, respectively. These are the temperatures estimated in Appendix A for laser power at the upper oscillation limit and at 500 mW, respectively.

At the upper limit of the oscillation range the laser power measured at the exit is 49 mW when the bath temperature is 1.65 K (see Table IV). As stated in Appendix A 4, 0.10 of the laser power is available to heat the crystal so the temperature rise is produced by ~ 5 mW. This is approximately the same as the microwave heating power produced by EPR and therefore the Nd^{3+} EPR microwave heating will produce further marked changes in the populations of the excited E and D states. These population changes result in the corresponding changes in fluorescence intensities that afford the means for optical detection of EPR at the higher laser powers and correspondingly higher temperatures.

The results of this mechanism for ODMR are illustrated in the ODMR row of Table VII and in Figs. 13 and 14. In the low power range the E_1 emissions show ODMR signals that are enhancements of the fluorescence intensity, accounted for by the mechanism described in Sec. I. In the "high power" range in which that mechanism is ineffective the shift of E population from the E_1 to higher energy states of the manifold, produced by microwave heating and EPR conditions, results in the deenhancement of the E_1 fluorescence intensity. If the population ratio, n_{E_2}/n_{E_1}, at the upper oscillation threshold for laser power were ~ 0.33 corresponding to a Boltzmann distribution at the estimated temperature, 25 K, a rise of another 10 K produced by EPR heating would change the ratio to ~ 0.45. This is an approximately 10% decrease in the population of the E_1 state giving an appreciable deenhancement of the E_1 fluorescence intensity. The population of the E_2 state would be increased by approximately 25% by this same 10 K increase in temperature producing an enhancement ODMR signal. Although quantitative values of temperatures and populations are not available it is very clear that the ODMR signals from E fluorescences in the laser high power range and the marked difference in their nature from that in the low power range are accounted for qualitatively by the EPR microwave heating of the crystal. The discussion just given for the case of E_2 ODMR also applies to the E_3 and E_4 emissions, and their observed enhancements by EPR microwave absorption are in agreement with expectations.

The situation with respect to ODMR for the D emissions is much more complicated. The proposed mechanism for populating the D states at higher temperatures has been outlined in Sec. IV B *1*. This proposed mechanism involves indirect paths of populating D states through energy transfer processes that become possible at higher temperatures because of thermal populating of the Z_2 level. $E_1, E_2, E_3 \rightarrow X, Y$ transitions then excite some of the Z_1 systems to D states by energy transfer processes. The EPR heating of the crystal increases the Z_2 population which in turn increases the D_1 and D_2 populations. If a Boltzmann population distribution existed at the upper oscillation limit for laser power, the previously made estimate of 25 K for the temperature would correspond to 0.0013 of the total Z population being in the Z_2 state. An additional 10 K temperature increase due to EPR microwave absorption would increase the Z_2 population by a factor of ~ 7, leading to enhancement of the D populations and their fluorescence emissions, in agreement with observations under most conditions. However, the mechanism of D fluorescence leads to complications described below, which may account for the exceptions mentioned in Sec. III C and shown in Fig. 15 for a small range of power just above the upper oscillation limit.

3. *D-level optical resonances*

There are 11 different possible matches between energies of $Z_2 \rightarrow D$ and $E \rightarrow X, Y$ transitions that may lead to the energy transfer required for D state fluorescence as described in Sec. IV B 1. Because of the different sizes of Zeeman splittings for the various levels involved in these energy transfers and their effects on the aforementioned energy matches that result in D fluorescence emissions, the changes in D fluorescence intensity when $|\mathbf{B}_0|$ is varied are complicated. It is clear that the multiple optical resonances shown in Figs. 14 and 18 and described in Sec. III C and the third column of Table VII, the second row, are to be expected on the basis of the preceding discussion.

4. *Decay of the ODMR signals*

In Sec. III C and in the fourth row of Table VII we have described the striking differences between the decays of the ODMR signals in the low power and high power regions, when microwave irradiation is terminated and laser irradiation and $|\mathbf{B}_0|$ are maintained constant.

For the low power region in which the ODMR signals are effected by the mechanism described above in Sec. I, Furrer and Hutchison[21] have described the factors influencing these decays, and the reader is referred to that paper for further discussion (see their Sec. IV). They point out that in the low power range there are three contributors to the redistribution of the populations of the

two Zeeman components of the ground Z_1 state after cessation of the microwave irradiation: (a) spin-lattice relaxation; (b) the carrying of Nd^{3+} ion population from the upper to the lower energy component by the continued optical pumping out of the lower component; and (c) for the special values $\frac{1}{2}$, 1, 2, 3, and 4 of $R \equiv {}^{Er}g/{}^{Ng}g$, the cross relaxation between Nd^{3+} and Er^{3+}. For $R \neq \frac{1}{2},1,2,3,4$ the population redistribution rate is determined mainly by the single contribution (b) because of the relatively very long spin-lattice $1/e$ time, ~ 1 s.[24] Thus the ODMR decay is single exponential in form with a $1/e$ time much shorter than that due to spin-lattice relaxation. For $R = \frac{1}{2},1,2,3,4$ the cross relaxation between Nd^{3+} and Er^{3+} is important and leads to nonexponential decay at the corresponding values of $\theta = \cos^{-1}(\hat{\mathbf{B}}_0 \cdot \hat{\mathbf{c}})$. At these angles the Nd^{3+}-Er^{3+} interaction affords an additional decay channel. This produces a value of τ in the relation,

$$I(t) = I(t_0)\exp[-(t-t_0)/\tau] ,$$

that is distinctly reduced from its value at nearby angles. Also, in the low power range, τ decreases as laser power increases because of the increased optical pumping rate.

In the high power range the populations of the Zeeman components of the ground crystal field states of Nd^{3+} are nearly equally populated and the same is true for Er^{3+}. Thus contribution (c) (see above) to the $1/e$ time for the ODMR decay is not present. So the decay is single exponential for all values of $\cos^{-1}(\hat{\mathbf{B}}_0 \cdot \hat{\mathbf{c}})$ and τ is constant, at constant laser power, for all values of this angle. The decay rate is determined almost entirely by the population redistribution produced in the ground state doublet by the continued optical pumping. The reason for the increase, listed in the fifth row of Table VII, in the value of τ as laser power is increased is not clear. It is possible that there are changes in branching ratios and transition probabilities for the various processes of the optical pumping cycle, produced by the appreciable increase in temperature as power is increased in the high power range. These may alter the population redistributions produced by the optical pumping in such a manner as to lead to the increase in τ.

C. Fluorescence after interruption of laser beam followed by continued irradiation

In Sec. III B we presented the results of experiments in which the laser beam was interrupted for various lengths of time and irradiation of the crystal resumed after the end of the interruption time while the $E_1 \rightarrow Y_1$ fluorescence intensity was continuously monitored. Although we do not know the precise form of the relationship between the $E_2 \rightarrow Y_1$ fluorescence intensity and the crystal temperature, we believe that, for a given pumping rate of the $Z_1 \rightarrow F_1$ transition in the laser power range employed, rises and falls in the $E_2 \rightarrow Y_1$ fluorescence intensity indicate, respectively, rises and falls in the crystal temperature.

In view of this the following interpretation of the results of these experiments is proposed. When the laser beam is interrupted the crystal cools and for sufficiently long interruption times and with sufficiently high starting laser powers it will cool to temperatures for which the $E_2 \rightarrow Y_1$ fluorescence intensity is greatly reduced. On resumption of irradiation of the crystal it is reheated to its original temperature in a time which depends on the length of the interruption time (on which the extent of cooling depends) and on the laser power (on which the rate of heating depends). Clearly it is expected that the time required to reheat the crystal and therefore to restore the initial fluorescence intensity increases for a given laser power as the interruption time is increased and the results plotted in Fig. 7 demonstrate such a trend. The results also indicate that the time required for the crystal to reach its equilibrium temperature on resumption of irradiation increases as the laser power is reduced. Unfortunately a more quantitative analysis is not possible because of the failure of attempts mentioned in Appendix A 2 to develop a method of determining the crystal temperature from fluorescence intensity measurements.

The interpretation of the pulse of fluorescence following resumption of irradiation of the crystal in the high power range reported in Sec. III B and shown in Fig. 9 is not as straightforward. It is likely that this phenomenon is closely related to the fluorescence intensity oscillations discussed in Sec. IV D. If, however, it is assumed that the fluorescence intensity detected after the end of the interruption time corresponds to the $E_2 \rightarrow Y_1$ fluorescence intensity for the temperature to which the crystal has cooled during the interruption, these results could, in principle, be used to give information about the crystal cooling rate during laser-beam interruption. For the reason already mentioned, detailed quantitative analysis is not possible, but if the assumption stated above is valid it follows that the crystal requires an interruption of the laser beam of approximately 10 s to cool to a temperature at which $E_2 \rightarrow Y_1$ fluorescence intensity is reduced to $\frac{1}{20}$ of its initial value at the stated laser power.

Using the sources of heat capacity and thermal conductivity data mentioned in Appendix A 4 and assuming that the impedance to heat flow from the crystal surface to the helium bath is provided by the thermal resistance of the fused silica only, it is estimated that the crystal would cool from 25 to 5 K in approximately 0.2 s. Therefore the interpretation given above is consistent with the suggestion made in Appendix A 4 that the solid-solid interface provides a large fraction of the impedance to heat flow.

D. Oscillations of fluorescence intensity

In Secs. III B and III C we described the oscillations of the intensities of fluorescence emissions that occur in the intermediate range of laser power. We conclude that this behavior is the result of temperature oscillations. The crystal temperature at the upper limit of the laser power range for oscillation has been estimated in Appendix A 3 to be ~ 25 K and we believe the temperature is oscillating between that value and a lower one characteristic of the low power range.

Evidence for this assumption of oscillating crystal tem-

perature is as follows. We have in Sec. III B reported the result that as laser power crosses the threshold into the intermediate power region, coming from the low power region, the E_1 fluorescence intensity falls to a lower value and then oscillates between that lower value and the greater intensity characteristic of the low power region. In contrast the E_2, E_3, and E_4 emission intensities increase as that threshold is crossed and then oscillate between this higher value and a zero value characteristic of the low power region. The mechanism for production of the E_1, E_2, E_3, and E_4 fluorescences has been discussed in Sec. IV A. The fact that E_1 intensities are lower in the high power than in the low power region follows from the temperature increase and corresponding E_1 population decrease in the high power region relative to the low power region. In Sec. IV A the E_1 population at the upper oscillation limit ($\sim$25 K) is estimated to be 0.69 of its low-temperature value and this results in a lowered E_1 fluorescence intensity. This effect of laser heating through the radiationless transitions and its effect on the fluorescence intensities have been discussed in earlier parts of Sec. IV. For E_2, E_3, and E_4 states the effect of increased temperature on population and intensity is opposite to that for E_1, the fraction of E population in the E_2 state being estimated to change from $\sim$0.00 in the low-temperature region to $\sim$0.31 at the upper oscillation limit and this results in an increased emission intensity. Thus the observed behaviors of the E fluorescences are to be expected if temperature oscillations that result in population oscillations are occurring, and they therefore provide evidence that this is the case.

The situation with respect to D fluorescence oscillations is more complicated because of the complex mechanism, discussed in Sec. IV B 1 for production of D fluorescence in the high power range. There is a very small range of power just above the oscillation limit in which, as noted in Sec. III C and seen in Fig. 15, there are exceptions to the general high power behavior of the D_1 and D_2 fluorescences that may not be obvious because of these complications. The similarity of the oscillation behavior of the D_1 fluorescence to that of the E_1 on entering the oscillation range from lower powers, although unexplained in as simple a way as for the E case, may be presumed to originate in the complexities referred to above. The changes in E_1, E_2, D_1, and D_2 intensities at the onset of oscillations are listed in Table V.

A second evidence of temperature oscillations is provided by the results reported near the end of Sec. III C and in Fig. 19 concerning the effect of EPR on the oscillations. We have shown in Sec. IV B 2 that the ODMR signals in the high power range may be accounted for by the heating of the crystal produced by microwave absorption under EPR conditions. The fact that the E_1 ODMR signal is, in the high power region, a deenhancement of fluorescence intensity rather than an enhancement (as is the case for the low power region) is a result of the higher temperature and the decrease in E_1 population produced by microwave heating under EPR conditions. The ODMR signal generated when microwave irradiation was initiated with $|\mathbf{B}_0|$ at the value of Nd^{3+} EPR, oscillated between the fluorescence enhancement characteristic of the low power lower temperature region and the deenhancement characteristic of the higher-temperature regime. This is the behavior to be expected if oscillations of crystal temperature are occurring. The D_1 fluorescence, which in a narrow laser power range just above the upper oscillation limit also gives an ODMR deenhancement signal, behaves in the same manner as just described for E_1. When microwave irradiation was initiated with $|\mathbf{B}_0|$ at the value for Er^{3+} EPR the effect was quite different. The behavior of the fluorescence described in Sec. III C and Fig. 19 is a complete annihilation of the oscillations by the establishment of EPR conditions that persists as long as Er^{3+} EPR absorption continues. (See Sec. III C for a detailed description of this behavior.) Whereas in the intermediate power region Nd^{3+} EPR produces a signal that oscillates between low power and high power character, Er^{3+} EPR stops the oscillation and locks the fluorescence at its high power value, an enhancement or a deenhancement, whichever is the high power behavior of the particular emission being observed. We have noted in Appendix B that the EPR microwave heating by Er^{3+} EPR absorption at the upper limit of the oscillation region is considerably greater than that for Nd^{3+} EPR. Thus the microwave heating by Er^{3+} EPR absorption when the laser power is anywhere in the oscillation range is able to push the system completely into the high power (i.e., high-temperature) region, whereas the smaller rate of heat input by Nd^{3+} EPR leaves the system still in an intermediate state with the ODMR signal oscillating. Further, when the laser power is in a range from $\sim$5 to 0 mW below the upper oscillation limit, Nd^{3+} EPR will also cause oscillations to cease.

Although the evidences for temperature oscillations are convincing we have no explanation of their source. It has been very tempting to interpret these oscillation phenomena as the result of processes similar to those that are operative in the case of oscillations of composition that occur in some cases during the temporal evolution of a chemically reacting mixture of various chemical species.[25] Of particular interest has been the work of Salnikov[26] who early discussed the simultaneous oscillations of temperature and of concentrations of chemical species in chemically reacting systems. He showed that in reacting systems in which reactions liberate heat and in which it is also true that the rates of the reactions are sensitive to temperature changes, the conditions sufficient for oscillations of both temperature and concentrations of chemical species may occur. The analogy to our oscillating fluorescence intensities is apparent. The fluorescence intensities monitor the populations of the states from which the emissions are occurring. These populations are produced by the pumping cycles such as those depicted in Fig. 3. Thus these populations are determined, among other things, by the rates of the radiationless processes which are the source of crystal heating. The rates of these radiationless processes are sensitive to the temperature changes that are produced by the heat that these processes themselves produce. Thus, in principle, conditions may be established in the optically pumped system

sufficient for production of oscillating populations of the states from which fluorescence emission occurs. It is also true for such thermokinetic chemical oscillations as those discussed by Salnikov[26] and subsequent workers[27] that there are found to be critical finite ranges of experimental parameters inside which sustained oscillations can occur. This is reminiscent of our system with its finite range of laser powers required for oscillations of fluorescence intensities.

We have been forced to abandon an interpretation along the lines of the preceding paragraph by certain experimental observations. When $|\mathbf{B}_0|$ is swept through the range of values spanning the region of optical resonance (see Sec. I), with laser power in the range of values for oscillations when $\cos^{-1}(\hat{\mathbf{B}}_0\cdot\hat{\mathbf{c}})$ has values as listed in Table IV, results such as those shown in Fig. 18 are obtained. It is clear that the oscillations were sustained throughout the entire field range, from 1000 to 12 000 G in some cases. As explained in Sec. I the optical pumping efficiency varies over a wide range of values during the scanning of this large interval of field values. This variation is sufficiently large that one would expect that for some part of the range of field covered the temperature would lie outside the limits required for oscillation. Nevertheless the oscillation is sustained throughout the whole field scan as shown in Fig. 18. This result seems to make an interpretation analogous to that of Salnikov for chemically reacting systems inapplicable in the present situation.

The same type of difficulty is encountered with respect to other possible sources of the oscillations that we have considered: for example, (a) Taconis pressure and thermal oscillations that often occur in vessels, tubes or cavities submerged in liquid helium;[28] or (b) He gas bubbles that may be formed and may oscillate at the surface of an object submerged in superfluid helium and in which heat is being generated by optical excitation.[29]

V. CONCLUSION

The work reported here represents a considerable extension of this laboratory's previous studies of the effects of EPR microwave absorptions by rare-earth ions dilutely substituted at La^{3+} sites in $LaCl_3$ crystals on their optical absorptions and emissions. The essential new feature of this research is the observation of the importance of the effects of the heating of the crystal by both optical and microwave absorption in experiments in which the Nd^{3+} transition,

$$Z_1,\ {}^4I_{9/2},\ \mu=\tfrac{5}{2}\rightarrow F_1,\ {}^2G_{9/2},\ \mu=\tfrac{1}{2}\ ,$$

is optically pumped with the nearly resonant 19 429.67-cm^{-1} Ar^+ laser emission and simultaneously the ground Z_1 Kramers doublet is pumped with resonant microwave radiation in the presence of a magnetic field. The heating of the crystal by the phonons produced in the radiationless transitions involved in the optical pumping cycles results in the populating of excited states and accounts for 17 D and E (Dieke notation) fluorescence emissions that are not observed when the crystal is at liquid-helium temperatures. Because of the crystal mounting techniques that are used in these experiments, involving encapsulation of the crystal in fused silica envelopes, these heating effects are particularly marked. In some of the crystals Er^+ ions are also present at La^{3+} sites. Either Nd^{3+} or Er^{3+} EPR and the associated spin-lattice relaxations of the ground Z_1 Kramers doublets produce a microwave heating in addition to that produced by the optical pumping. This produces striking effects on the intensities of the 28 fluorescence emissions investigated in this work and thus affords a new mechanism for ODMR of the rare-earth ions. For those emissions from excited states that are lowest in energy in a given manifold and whose populations are decreased by the redistribution effected by microwave heating, EPR markedly decreases the intensity of the fluorescence. For the higher states of the manifold there is an enhancement of the intensity of their optical emissions. This mechanism for ODMR produces optical signals strikingly different from those previously studied which resulted from the changes in the populations of the two components of the ground Z_1 doublet that were produced by microwave absorption. There are also large changes with temperature in the characters of the decays of the ODMR signals when microwave irradiation is terminated. These are understandable on the basis of this new mechanism.

We have considered several mechanisms for the production of the temporal oscillations of the intensities of the 28 Nd^{3+} fluorescences studied in this work that occur for constant intensity laser irradiation in the absence of external magnetic fields. None of them accounts for the observed features of this interesting phenomenon. It is very clear, however, that these oscillations of emission intensity are accompanied by crystal temperature oscillations and corresponding oscillations of populations of emitting states. The observed changes in the oscillations when EPR conditions are met are consistent with the interpretation that the fluorescence oscillations are the result of oscillations of state population distributions between those characteristic of low laser powers and those associated with the higher temperatures produced at higher laser powers.

ACKNOWLEDGMENTS

We gratefully acknowledge the design and construction by Clark E. Davoust and Karolis Avizienis of the equipment used in the experiments. This research has been supported by the National Science Foundation and the National Institutes of Health Grant No. PHS 5-R01 GM-21668. P.M.M. thanks the IBM Corporation for additional financial support.

APPENDIX A: EVIDENCE FOR MARKED INCREASE OF CRYSTAL TEMPERATURE WITH INCREASING LASER POWER

1. Linewidth of the optical resonance versus laser power

In Table II are summarized the results of measurements of the full width of the optical resonance at half maximum amplitude for several different laser powers.

According to the discussion of the optical resonance given in Sec. I the difference $\Delta H_{1/2}$ in values of $|\mathbf{B}_0|$ at the half-maximum points is determined by the wave number width of the crystal's optical absorption. In the third column of Table II are given the values of $[\Delta H_{1/2}({}^{g}g + {}^{e}g)|\mu_B|]/2hc$. They are in agreement with expected values of optical absorption width and expected increases of optical absorption width with increasing temperature.

2. The ratio of intensities of different fluorescence emissions versus laser power

In Table VI are listed the values of the fluorescence intensity ratios I_{E_2}/I_{E_1} and $(I_{D_2}+I_{D_3})/I_{D_1}$, versus laser power. The D_2 and D_3 emissions were not well resolved. The increase in these ratios with increase of laser powers indicates an increase in the populations of the higher energy states of the E and D manifolds as laser power is increased. This in turn is evidence for an appreciable increase in the crystal temperature. In view of the fact that lifetimes (see Table I) in the E_2, D_2, and D_3 states, of order 30–50 μs, are long compared with thermal equilibration times, less than 1 μs, we expect populations of states of the E and D manifolds to approach Boltzmann distributions characteristic of a crystal temperature. If oscillator strengths were known these data could in principle yield the values of the population ratios and therefore values of the crystal temperatures when combined with Dieke's[4] measured energy level values. Because they are not known we tried a number of schemes which eliminated the need for the values of oscillator strengths by making comparisons of E manifold intensity ratios and D manifold ratios, and assuming that (a) there is a uniform crystal temperature that is the same for both E and D state systems; (b) that oscillator strengths do not vary rapidly with temperature; and (c) that ions remain a long enough time in the E and D manifolds for Boltzmann distributions to be established. None of these attempts gave consistent results, presumably because not all of these assumptions are justified. However, the observed changes in the intensity ratios given in Table VI clearly indicated appreciable increases in the populations of the higher E and D levels produced by crystal heating.

3. The linewidth of the ODMR signals

Figure 16 presents the measured values of the ODMR linewidths as a function of laser power. The marked increases in width as laser power is increased are indicative of increases in phonon-assisted broadening and decreasing spin-lattice relaxation times as a result of increasing temperature of the crystal. In principle, the ODMR widths shown in Fig. 16 should permit a determination of the crystal temperature as a function of laser power. Gray and Stapleton[30] have measured EPR linewidths for Nd^{3+} in $LaCl_3$ as a function of temperature of the crystal from 2.7 to 29 K above which they could not observe EPR. At temperatures above 2.7 K they used the Stoneham[31] deconvolution formula for first derivatives of the line shapes and the measured lowest temperature Gaussian width to extract the values of the phonon-assisted Lorentzian contributions at the higher temperatures. In our present case, a measurement of the 1.6-K EPR linewidth together with the extensive convolution tables of Posener[32] should permit extraction of the phonon-assisted contribution to our measured ODMR linewidths as a function of laser power. Comparison with the data of Gray and Stapleton[30] would then give values for the temperature of the crystal. We were not successful with such an attempt to find an accurate value of temperature, mainly due to the fact that it was not possible to obtain an accurate low-temperature Gaussian width due to the complicated structures of the EPR signals caused by the relatively high concentrations of rare-earth ions in our crystals. If we assume the not very accurate value, 25 G, for the low-temperature Gaussian EPR full width at half maximum, and use the measured D_1-Z_4 ODMR signal width, 57 G, shown by the solid line in Fig. 16, at the upper limit of the oscillation range, then the procedure outlined just above gives the value 46 G for the phonon-assisted Lorentzian contribution to the width. From the data of Gray and Stapleton this corresponds to the temperature, 25 K, for the crystal. At higher laser powers the ODMR linewidths are so large that the deconvolution correction is negligible. For a laser power, 500 mW, the quadratic fit shown in Fig. 16 for the D_1-Z_4 signal for Nd^{3+} yields the value, 302 G, for the width at 500-mW laser power. This corresponds to the temperature, 35 K. For the Er^{3+} D_1-Z_4 signal the quadratically extrapolated width at 500 mW is 671 G which corresponds to 30 K.

4. Thermal properties of $LaCl_3$ and amorphous SiO_2

In Sec. III A we have pointed out that 0.75 of the power measured at the laser exit reached the crystal surface in our experiments. The measured absorptance reported there was $\sim$0.50. Radiationless transitions dissipated $\sim$0.25 of the absorbed energy. Thus 0.10 of the laser power is given off as heat and 0.28 as fluorescence emission. (It is laser power measured at the laser exit that is plotted as abscissa in Figs. 11, 16, and 17.) Sommers and Westrum[33] have measured the heat capacity of $LaCl_3$ from 5 to 350 K. Values of the heat capacity and thermal conductivity of amorphous SiO_2 are given in the tables of Thermophysical Properties of Matter.[34] Thus there is sufficient information available to calculate the rate of rise of temperature of the encapsulated crystal and the temperature attained by the crystal in the steady state in which the 0.10 of the laser power producing heat in the crystal is equal to the loss through the silica tube to the helium, provided one makes the assumption that the impedance to heat flow from the crystal surface to the helium bath is provided by the thermal conductance of the silica tube only. Our finding was that the difference in temperature between the inside and outside tube walls, the outside wall assumed to be at the helium bath temperature, required to conduct the 0.10 of the laser power, resulted in an inside wall temperature much lower than the temperature of the crystal estimated from linewidths. Even allowing for the crudeness of the estimate of temperature from linewidths it is very clear that a large frac-

tion of the impedance to heat flow is provided by the solid-solid interface. This effect is not sufficiently well known to make even a crude estimate of crystal temperature based only on physical properties of crystal and silica tube and known laser power.

APPENDIX B: MICROWAVE POWER ABSORBED BY CRYSTAL

The microwave power, dW/dt, dissipated by the Nd^{3+} EPR may be estimated from the relation

$$\frac{dW}{dt}=\frac{Nw_e h\nu}{1+2w_e\tau_1}\tanh\left[\frac{h\nu}{2kT_0}\right], \tag{8}$$

which holds under steady-state conditions of microwave absorption by Nd^{3+} ions and energy dissipation in the crystal by spin-lattice relaxation. N is the number of Nd^{3+} ions in the crystal, ν is the microwave frequency, T_0 is the crystal temperature, w_e is the rate at which transitions between the Zeeman doublet components are induced by the microwave field, and τ_1 is the spin-lattice relaxation time. w_e is given by

$$w_e=\gamma^2 B_1^2/16\pi\Delta\nu_{1/2}, \tag{9}$$

in which γ is the gyromagnetic ratio, B_1 is the microwave magnetic field at the crystal, and $\Delta\nu_{1/2}$ is the frequency half width at half maximum absorption amplitude. The value of γ is taken to be that for $\cos^{-1}(\hat{\mathbf{B}}_0\cdot\hat{\mathbf{c}})=\pi/4$. The $\Delta\nu_{1/2}$ value is obtained from the quadratic least-squares fit to the experimental data shown as a solid line in Fig. 16. B_1 is calculated from the cavity Q, microwave power dissipated in the cavity, the cavity volume and the microwave frequency. Values of these quantities are given in Sec. II C. The value of τ_1 for Nd^{3+} in $LaCl_3$ as a function of crystal temperature has been measured by Mangum and Hudson.[24] The value of N is determined by the information given in Sec. II A. With the insertion of these values into Eqs. (8) and (9) we find ~ 7 and ~ 10 mW to be the values of the microwave power dissipated as heat in the crystal by spin-lattice relaxation at crystal temperatures, 25 and 35 K, respectively. These are the estimated crystal temperatures (based on Nd^{3+} ODMR linewidths) for (a) laser power at the upper oscillation limit and (b) for laser power, 500 mW, respectively (see Appendix A 3). These powers are approximately the same as the ~ 5-mW laser power that is being dissipated in the crystal at the upper oscillation threshold and that has heated the crystal to ~ 25 K and produced the altered populations described in Sec. IV A.

A numerical estimation procedure similar to that just described, when applied to Er^{3+}, with data taken from the same sources, yields the values, ~ 20 mW and ~ 9 mW, for the microwave power dissipated as heat in the crystal by Er^{3+} EPR absorption of microwave energy at the upper oscillation level and at 500 mW of laser power, respectively.

*Present address: IBM Research, Thomas J. Watson Research Center, Box 218, Yorktown Heights, NY 10598.
†Present address: The Department of Physical Chemistry, University of Cambridge, Lensfield Road, Cambridge CB2 1EP, United Kingdom.

[1]W. H. Zachariasen, J. Chem. Phys. **16**, 254 (1948).
[2]B. Morosin, J. Chem. Phys. **49**, 3007 (1968).
[3]E. H. Carlson and G. H. Dieke, J. Chem. Phys. **29**, 229 (1958).
[4]G. H. Dieke, *Spectra and Energy Levels of Rare Earth Ions in Crystals* (Interscience, New York, 1968).
[5]E. H. Carlson and G. H. Dieke, J. Chem. Phys. **34**, 1602 (1961).
[6]G. E. Barasch and G. H. Dieke, J. Chem. Phys. **43**, 988 (1965).
[7]G. H. Dieke and S. Singh, J. Chem. Phys. **35**, 555 (1961).
[8]W. B. Gandrud and H. W. Moos, J. Chem. Phys. **49**, 2170 (1968).
[9]N. Krasutsky and H. W. Moos, Phys. Rev. B **8**, 1010 (1973).
[10]N. Pelletier-Allard and R. Pelletier, J. Phys. (Paris) **41**, 861 (1980).
[11]C. A. Moore, Phys. Rev. B **13**, 1925 (1976).
[12]C. A. Moore and R. A. Satten, Phys. Rev. B **7**, 1753 (1973).
[13]E. Y. Wong, J. Chem. Phys. **34**, 1989 (1961).
[14]C. A. Hutchison, Jr. and E. Y. Wong, J. Chem. Phys. **29**, 754 (1958).
[15]A. Abragam and B. Bleaney, *Electron Paramagnetic Resonance of Transition Ions* (Clarendon, Oxford, 1970).
[16]R. C. Clarke and C. A. Hutchison, Jr., Phys. Rev. Lett. **27**, 638 (1971).
[17]J. P. Hessler and C. A. Hutchison, Jr., Phys. Rev. B **8**, 1822 (1973); J. P. Hessler (unpublished).
[18]J. M. Clemens and C. A. Hutchison, Jr., Phys. Rev. B **28**, 50 (1983).
[19]C. A. Hutchison, Jr., J. M. Clemens, J. P. Hessler, and E. D. Liu, Semicond. Insulators **3**, 61 (1978).
[20]C. A. Hutchison, Jr. and E. D. Liu, J. Lumin. **12/13**, 665 (1978).
[21]R. Furrer and C. A. Hutchison, Jr., Phys. Rev. B **27**, 5270 (1983).
[22]Th. Foerster, Ann. Phys. **2**, 55 (1948).
[23]J. H. Anderson and C. A. Hutchison, Jr., Phys. Rev. **97**, 76 (1955).
[24]B. W. Mangum and R. P. Hudson, J. Chem. Phys. **44**, 704 (1966).
[25]*Oscillations and Traveling Waves in Chemical Systems*, edited by R. J. Field and Maris Burger (Wiley, New York, 1985).
[26]I. Ye. Salnikov, Zh. Fiz. Khim. **23**, 258 (1949).
[27]See, for example, J. S. Griffiths, *The Theory of Transition Metal Ions* (Cambridge, University Press, Cambridge, England, 1961), Chap. 15.
[28]K. W. Taconis, Physica **15**, 733 (1949), see footnote p. 738; H. A. Kramers, Physica **15**, 971 (1949).
[29]M. Greenstein and J. P. Wolfe, J. Phys. Colloq. **C6**, 42 (1981).
[30]W. T. Gray IV and H. J. Stapleton, Phys. Rev. B **9**, 2864 (1974).
[31]A. M. Stoneham, J. Phys. D **5**, 670 (1972).
[32]D. W. Posener, Aust. J. Phys. **12**, 670 (1959).
[33]J. A. Sommers and E. F. Westrum, Jr., J. Chem. Thermodyn. **8**, 1115 (1976).
[34]*Thermophysical Properties of Matter*, edited by Y. S. Touloukian (IFI/Plenum, New York, 1970), Vol. 5.